Journal of Arrhythmia 29 (2013) 305–307

Contents lists available at ScienceDirect

Journal of Arrhythmia

journal homepage: www.elsevier.com/locate/joa

Commentary

Paradigm shifts in the genetics of inherited arrhythmias: Using next-generation sequencing technologies to uncover hidden etiologies

Naomasa Makita, MD, PhD*

Department of Molecular Physiology, Nagasaki University Graduate School of Biomedical Sciences, 1-12-4 Sakamoto, Nagasaki 852-8523, Japan

ARTICLE INFO

Article history:
Received 9 August 2013
Received in revised form
9 September 2013
Accepted 11 September 2013
Available online 31 October 2013

Keywords:
Next-generation sequencing
Exome
Calmodulin
Long QT syndrome
Inherited arrhythmia

Long QT syndrome (LQTS), a rare inheritable arrhythmia first described by Romano and Ward et al. in the 1960s, is characterized by the prolongation of the QT interval on surface ECGs and an increased risk of potentially fatal ventricular arrhythmias, especially torsade de pointes [1]. In 1995, after years of extensive clinical investigation and linkage analysis, several research groups, including Keating et al., successfully identified three distinct LQTS phenotypes (LQT1, LQT2, and LQT3) associated with mutations in genes encoding plasma membrane ion channels (*KCNQ1*, *KCNH2*, and *SCN5A*, respectively) [2–4]. These seminal studies motivated further extensive genetic screening in LQTS patients using a candidate gene approach and functional analyses of the mutant genes. These efforts provided evidence that ion channel genes represent the genetic basis for several other arrhythmogenic syndromes that occur in the structurally intact heart, often referred to as idiopathic ventricular fibrillation. At present, 13 genes responsible for LQTS have been identified. Approximately 90% of the genotyped LQTS subjects belong to the three major subtypes (LQT1-3) [5] in which numbers of distinct genotype-specific clinical characteristics have been demonstrated, including T-wave morphology [6], triggers for cardiac events [7], response to the epinephrine provocation test [8] and drug therapy [9]. Genetic testing for known arrhythmia susceptibility genes has become the standard-of-care for a number of disorders, including LQTS. Considering the remarkable progress of research in this area, there is no doubt that 1995 was the year in which genetic technologies experienced a paradigm shift with respect to both the understanding and clinical management of inherited arrhythmias. However, it should be noted that despite the rapid progress in understanding the genetic basis, the etiology still remains unknown in approximately 20% of LQTS conditions [10]. Therefore, additional studies are needed to reveal the missing heritable factors associated with these syndromes.

Traditionally, DNA sequence information has been elucidated using Sanger sequencing, but this method is limited by the amount of DNA that can be processed at a given time and by the read length (average 800 base pairs). Although the Human Genome Project completed the sequencing of the entire human genome in 2001 using Sanger sequencing, it took 13 years of effort at an estimated cost of $2.7 billion. Now, next-generation sequencing (NGS), a revolutionary new genetic technology, has enabled whole genomes to be sequenced over a period of a few days at projected costs of less than $10,000. This technology involves massively parallel sequencing of clonally amplified or single DNA molecules that are spatially separated in a flow cell.

To date, the genes responsible for disease in more than 3000 Mendelian disorders have yet to be identified. NGS opens up exciting new possibilities of discovering the genes associated with these monogenic disorders. Classical strategies involve linkage analysis in families with known shared genetic heritage by identifying candidate genomic regions encompassing the gene

* Tel.: +81 95 819 7031; fax: +81 95 819 7911.
E-mail address: makitan@nagasaki-u.ac.jp

http://dx.doi.org/10.1016/j.joa.2013.09.001

with the causative mutation. After narrowing the interval with additional families/probands, a candidate gene approach or an approach of systematically sequencing the genes located within the interval can be implemented. Genome-wide association studies (GWAS), which use single nucleotide polymorphisms (SNPs), can significantly expedite the linkage analysis by narrowing the regions of interest for further directed sequencing. GWAS have been applied in the cardiac electrophysiological field and over 100 traits have been identified for common diseases such as atrial fibrillation, or ECG parameters such as PR, QT, and RR intervals and QRS durations [11]. These conventional approaches are costly and time-consuming, and their success in identifying the causative genetic variants has been variable, mainly because of the small numbers of affected individuals for a given Mendelian disease and also possibly due to locus heterogeneity. However, a recent multicenter GWAS study involving our group has shown that common genetic variation can have a strong impact on the predisposition of rare diseases such as Brugada syndrome [12].

Deep resequencing of all human genes for the discovery of allelic variants could potentially identify genes whose dysfunction underlies any given rare monogenic disease when a shared genetic heritage is not readily available. Protein-coding exons represent only approximately 1% of the entire 30-Mbp human genome but are estimated to harbor approximately 85% of the mutations that cause largely govern the expression of disease-related traits. Indeed, most Mendelian disorders are thought to be attributable to exonic mutations or splice-site mutations that alter the amino acid sequence of the affected gene. Therefore, whole exon sequencing (WES) (or exome sequencing) using NGS platforms will allow vastly higher sequence coverage with considerably less raw sequence and lower cost than whole genome sequencing. Since its first application in 2008, a number of previously unidentified monogenic traits have been discovered using WES techniques [13–15]. These results have been achieved frequently using a limited number of patients with genetic defects in both autosomal dominant [14] and recessive [15] disorders. The implementation of NGS technology in cardiology is expected to bring a second paradigm shift in how clinical cardiologists diagnose patients and how researchers investigate both common and rare disorders. Potentially, all causative variants and genes and their relation to phenotypes in Mendelian disorders will be uncovered in the very near future. Such technologies should also enable us to identify all the variants in an individual's personal genome and, in particular, to highlight clinically relevant alleles. Whole genome sequencing is expected to produce a major shift in clinical practice in terms of diagnosis and understanding of cardiovascular diseases, which will ultimately enable personalized medicine based on an individual's genome.

Crotti et al. recently identified two novel disease-causing genes responsible for sudden unexplained death syndrome using WES [16]. They studied two unrelated infants with recurrent cardiac arrest and dramatically prolonged QTc intervals who were both born to healthy parents. The probands were confirmed in advance to be negative for mutations in major LQTS genes *KCNQ1*, *KCNH2*, *SCN5A*, *KCNE1*, and *KCNE2*. Applying WES to the two unrelated probands and their healthy parents, they searched for *de novo* genetic variants and found *de novo* mutations in either *CALM1* or *CALM2*, which encode calmodulin. To validate these WES results, they performed follow-up genetic screening of the calmodulin genes (*CALM1*, *CALM2*, and *CALM3*) on an independent cohort of 82 subjects who had congenital LQTS without a known genetic cause. They identified two individuals from this cohort who also displayed variations in calmodulin; one individual harbored the same mutation in *CALM1* as that seen in proband 1, and the other individual had a novel missense mutation in *CALM1*. The mutations altered residues in, or adjacent to, critical calcium binding loops in the calmodulin carboxyl-terminal domain. To determine the functional consequences of calmodulin mutations, they measured the Ca^{2+} binding activities of the recombinant calmodulin proteins in bacteria and confirmed that three mutations have significantly reduced Ca^{2+} affinity in the C domain.

The discovery of pathological variants in calmodulin has raised a variety of interesting and novel research questions. First, the observations by Crotti et al. illustrate the genotypic and phenotypic heterogeneity of calmodulin mutations. The mutant carriers in the study by Crotti et al. presented with early-onset life-threatening cardiac arrhythmias, prolonged QT intervals, and neurodevelopmental delay. Studies by other groups showed that mutations in *CALM1* may be linked to catecholaminergic polymorphic ventricular tachycardia with [17] or without [18] prolonged QT intervals. Furthermore, although the three calmodulin genes (*CALM1*, *CALM2*, *and CALM3*) are dispersed in the genome and encode identical calmodulin polypeptides, the phenotype variants exhibit considerable differences in severity of clinical phenotype. This phenotypic variability may suggest that the cellular distribution, gene dosage, or function of each calmodulin gene may not be equivalent. Although the authors did not address this issue, it will be intriguing to identify the molecular targets of calmodulin in the heart that underlie the action potential prolongation, as well as the predisposition to lethal arrhythmias. Clearly, more extensive experimental work, including studies of genetically engineered animals, is required to address these questions, to refine current disease classifications, and to learn more about the genomic origins of these and other diseases.

NGS technologies have the potential to uncover the hidden etiologies of many diseases; however, such technologies are a "double edged sword" because investigators leading clinical sequencing efforts may face serious ethical issues. They may unintentionally find a life-threatening genetic variation in a patient who is unrelated to the project, or they may question the decision whether they should provide the genetic information to family members in the event that a patient dies.

Conflict of interest

There is no conflict of interest related to this article.

References

[1] Keating MT. The long QT syndrome: a review of recent molecular genetic and physiologic discoveries. Medicine (Baltimore) 1996;75:1–5.
[2] Wang Q, Curran ME, Splawski I, et al. Positional cloning of a novel potassium channel gene: KVLQT1 mutations cause cardiac arrhythmias. Nat Genet 1996;12:17–23.
[3] Curran ME, Splawski I, Timothy KW, et al. A molecular basis for cardiac arrhythmia: HERG mutations cause long QT syndrome. Cell 1995;80:795–803.
[4] Wang Q, Shen J, Splawski I, et al. *SCN5A* mutations associated with an inherited cardiac arrhythmia, long QT syndrome. Cell 1995;80:805–11.
[5] Cerrone M, Priori SG. Genetics of sudden death: focus on inherited channelopathies. Eur Heart J 2011;32:2109–18.
[6] Moss AJ, Zareba W, Benhorin J, et al. ECG T-wave patterns in genetically distinct forms of the hereditary long QT syndrome. Circulation 1995;92:2929–34.
[7] Schwartz PJ, Priori SG, Spazzolini C, et al. Genotype-phenotype correlation in the long-QT syndrome: gene-specific triggers for life-threatening arrhythmias. Circulation 2001;103:89–95.
[8] Shimizu W, Noda T, Takaki H, et al. Diagnostic value of epinephrine test for genotyping LQT1, LQT2, and LQT3 forms of congenital long QT syndrome. Heart Rhythm 2004;1:276–83.
[9] Vincent GM, Schwartz PJ, Denjoy I, et al. High efficacy of β-blockers in long-QT syndrome type 1: contribution of noncompliance and QT-prolonging drugs to the occurrence of ß-blocker treatment failures. Circulation 2009;119:215–21.
[10] Schwartz PJ, Ackerman MJ, George Jr. AL, et al. Impact of genetics on the clinical management of channelopathies. J Am Coll Cardiol 2013;62:169–80.
[11] Milan DJ, Lubitz SA, Kaab S, et al. Genome-wide association studies in cardiac electrophysiology: recent discoveries and implications for clinical practice. Heart Rhythm 2010;7:1141–8.

[12] Bezzina CR, Barc J, Mizusawa Y, et al. Common variants at *SCN5A-SCN10A* and *HEY2* are associated with Brugada syndrome, a rare disease with high risk of sudden cardiac death. Nat Genet 2013;45:1044–9.
[13] Shendure J, Ji H. Next-generation DNA sequencing. Nat Biotech 2008;26:1135–45.
[14] Ng SB, Bigham AW, Buckingham KJ, et al. Exome sequencing identifies *MLL2* mutations as a cause of Kabuki syndrome. Nat Genet 2010;42:790–3.
[15] Worthey EA, Mayer AN, Syverson GD, et al. Making a definitive diagnosis: successful clinical application of whole exome sequencing in a child with intractable inflammatory bowel disease. Genet Med 2011;13:255–62.
[16] Crotti L, Johnson CN, Graf E, et al. Calmodulin mutations associated with recurrent cardiac arrest in infants. Circulation 2013;127:1009–17.
[17] Marsman RF, Barc J, Beekman L, et al. A mutation in *CALM1* encoding calmodulin causes sudden cardiac death in childhood and adolescence. Heart Rhythm 2013;10:S395–6.
[18] Nyegaard M, Overgaard MT, Søndergaard MT, et al. Mutations in calmodulin cause ventricular tachycardia and sudden cardiac death. Am J Hum Gen 2012;91:703–12.

Circulation Journal
Official Journal of the Japanese Circulation Society
http://www.j-circ.or.jp

ORIGINAL ARTICLE
Arrhythmia/Electrophysiology

Novel *SCN3B* Mutation Associated With Brugada Syndrome Affects Intracellular Trafficking and Function of Nav1.5

Taisuke Ishikawa, BSc; Naohiko Takahashi, MD; Seiko Ohno, MD; Harumizu Sakurada, MD; Kazufumi Nakamura, MD; Young Keun On, MD; Jeong Euy Park, MD; Takeru Makiyama, MD; Minoru Horie, MD; Takuro Arimura, PhD; Naomasa Makita, MD; Akinori Kimura, MD

Background: Brugada syndrome (BrS) is characterized by specific alterations on ECG in the right precordial leads and associated with ventricular arrhythmia that may manifest as syncope or sudden cardiac death. The major causes of BrS are mutations in *SCN5A* for a large subunit of the sodium channel, Nav1.5, but a mutation in *SCN3B* for a small subunit of sodium channel, Navβ3, has been recently reported in an American patient.

Methods and Results: A total of 181 unrelated BrS patients, 178 Japanese and 3 Koreans, who had no mutations in *SCN5A*, were examined for mutations in *SCN3B* by direct sequencing of all exons and adjacent introns. A mutation, Val110Ile, was identified in 3 of 178 (1.7%) Japanese patients, but was not found in 480 Japanese controls. The *SCN3B* mutation impaired the cytoplasmic trafficking of Nav1.5, the cell surface expression of which was decreased in transfected cells. Whole-cell patch clamp recordings of the transfected cells revealed that the sodium currents were significantly reduced by the *SCN3B* mutation.

Conclusions: The Val110Ile mutation of *SCN3B* is a relatively common cause of *SCN5A*-negative BrS in Japan, which has a reduced sodium current because of the loss of cell surface expression of Nav1.5. (*Circ J* 2013; **77:** 959–967)

Key Words: Brugada syndrome; Electrophysiologic study; Genetics; Ion channels; Sodium

Brugada syndrome (BrS) is a cardiac channelopathy characterized by specific findings, such as accentuated J wave and ST-segment elevation in the right precordial leads on ECG, in the absence of structural heart diseases.[1–3] BrS patients sometimes suffer from syncope, and have a risk of sudden cardiac death caused by rapid polymorphic ventricular tachycardia or ventricular fibrillation.[1–3] Approximately 35% of BrS patients have a family history of the disease, which is consistent with the autosomal dominant inheritance, and mutations in 12 different genes have been reported as associated with BrS, of which the majority are mutations in *SCN5A* encoding a large subunit of the cardiac sodium channel Nav1.5.[3–12] The prevalence of BrS in East Asia including Japan is much higher, reaching 1 in 1,000–2,000, than the worldwide prevalence of approximately 1 in 10,000.[13–15]

Editorial p900

In cardiomyocytes, 5 distinct sodium channel β-subunits, Navβ1, Navβ1b, β2, β3 and β4, are known to be expressed. In particular, Navβ1 and Navβ3, encoded by *SCN1B* and *SCN3B*, are abundantly expressed, and these auxiliary β-subunits and a pore-forming subunit, Nav1.5, comprise the cardiac sodium channel complex.[4,16] Inward sodium current (I_{Na}) generated by the sodium channel complex is crucial for the cardiac action potential,[16,17] and functional alterations of I_{Na} caused by gene mutations have been reported in a wide range of arrhythmias, including long QT syndrome,[18] idiopathic ventricular fibrillation (IVF),[19] sudden infant death syndrome (SIDS),[20] and atrial fibrillation (AF).[21] In BrS patients, disease-causing mutations were found not only in *SCN5A* but also in the genes

Received August 1, 2012; revised manuscript received October 13, 2012; accepted November 16, 2012; released online December 21, 2012 Time for primary review: 35 days

Department of Molecular Pathogenesis, Medical Research Institute, and Division of Genetic Regulation, Graduate School of Medical and Dental Sciences, Tokyo Medical and Dental University, Tokyo (T.I., T.A., A.K.); Department of Laboratory Examination and Diagnostics, Oita University, Oita (N.T.); Department of Cardiovascular and Respiratory Medicine, Shiga University of Medical Science, Otsu (S.O., M.H.); Department of Cardiology, Tokyo Metropolitan Hiroo Hospital, Tokyo (H.S.); Department of Cardiovascular Medicine, Okayama University Graduate School of Medicine, Dentistry and Pharmaceutical Sciences, Okayama (K.N.); Department of Cardiovascular Medicine, Kyoto University Graduate School of Medicine, Kyoto (T.M.); Department of Molecular Pathophysiology, Nagasaki University Graduate School of Biomedical Sciences, Nagasaki (N.M.), Japan; and Division of Cardiology, Samsung Medical Center, Sungkyunkwan University School of Medicine, Seoul (Y.K.O., J.E.P.), Korea

Mailing address: Akinori Kimura, MD, PhD, Department of Molecular Pathogenesis, Medical Research Institute, Tokyo Medical and Dental University, 1-5-45 Yushima, Bunkyo-ku, Tokyo113-8510, Japan. E-mail: akitis@mri.tmd.ac.jp

ISSN-1346-9843 doi:10.1253/circj.CJ-12-0995

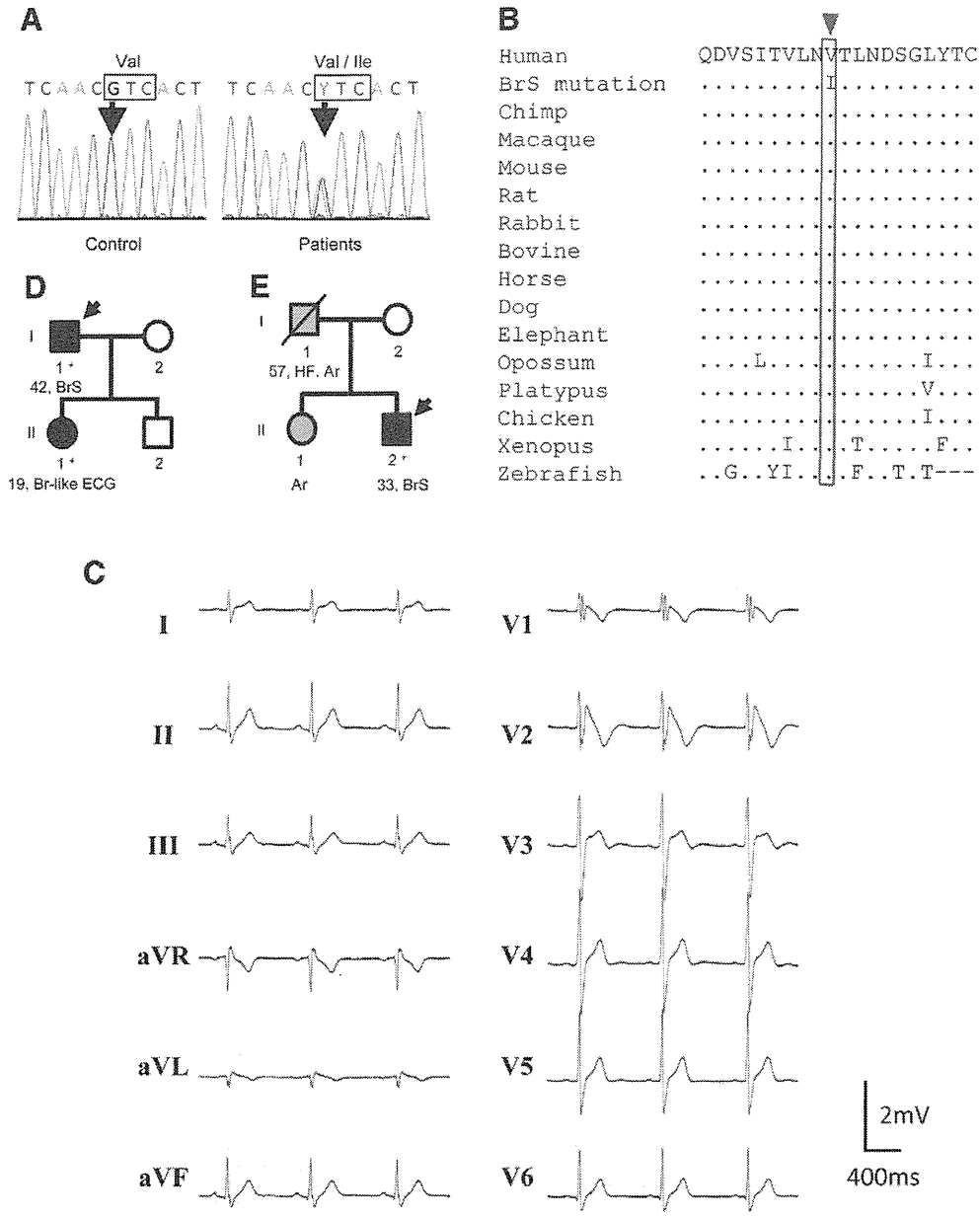

Figure 1. Mutational analysis of *SCN3B* in Brugada syndrome (BrS). (**A**) Direct sequencing analysis of exon 3 in a control (**Left**) and a patient, BrS-H-1 (**Right**), shows that the patient was heterozygous for GTC and ATC (Ile) at codon 110, where the control was homozygous for GTC (Val). The same pattern was obtained from the other proband patients, BrS-O-1 and BrS-S-1, as well as from BrS-O-2 who was a daughter of BrS-O-1 (**Table 1**). (**B**) Amino acid sequences of Navβ3 from various species aligned with the V110I mutation. (**C**) Representative ECG recording from BrS-O-1 shows typical coved-type ST-segment elevation in leads V1–2. Pedigrees of BrS families with the V110I mutation: BrS-O-1 (**D**) and BrS-S-1 (**E**). Squares and circles indicate male and female, respectively. Filled and open symbols represent affected and unaffected individuals, respectively. Shaded symbols indicate subjects with undefined arrhythmia (Ar). Arrows indicate the proband patients. Presence of the mutation is noted as +. Ages at blood sampling or death are indicated. HF, heart failure.

encoding modifier proteins of Nav1.5, which causes functional loss of I_{Na}.[8,12,22–25] Among the modifier proteins, Navβ3, which does not form the ion-conducting pore, modifies the function of Nav1.5 by modulating channel gating and increasing the cell surface expression of Nav1.5,[26] and hence *SCN3B* mutations could be responsible for BrS. Nevertheless, there is only 1 report of a *SCN3B* mutation, Leu10Pro, in an American patient with BrS,[23] although some other *SCN3B* mutations have been reported in other hereditary arrhythmias, including IVF,[27] SIDS,[28] and AF.[29,30]

We report a *SCN3B* mutation, Val110Ile, found in 3 unrelated Japanese BrS patients. Functional studies in transfected cells demonstrated that the mutation decreased the cell surface expression of Nav1.5 and reduced the peak current of the I_{Na}.

Table 1. Clinical Phenotypes of Individuals Carrying the *SCN3B* Val110Ile Mutation

ID	Age (years)/Sex	ST-elevation type	Symptoms	Family history of arrhythmia/SCD	ICD	EPS
BrS-O-1	42/M	Coved	Symptomatic	Yes	Yes	VF
BrS-O-2	19/F	Coved	Asymptomatic	Yes	No	–
BrS-S-1	33/M	Saddleback	Asymptomatic	Yes	No	NSVT
BrS-H-1	51/M	Coved	Syncope	No	No	–

BrS, Brugada syndrome; EPS, electrophysiologic study; ICD, implantable cardioverter defibrillator; NSVT, non-sustained ventricular tachycardia; SCD, sudden cardiac death; VF, ventricular fibrillation.

Methods

Subjects

We studied 178 genetically unrelated Japanese and 3 Korean patients with BrS. Age at the diagnosis of 145 male patients was 45.3±15.7 (range 7–76) years, and that of the 17 female patients was 46.8±17.3 (range 11–72) years. Episodes of syncope and/or arrhythmia had occurred in 93 patients, but the others were asymptomatic. There was a family history of sudden death and/or arrhythmias for 19 patients, but nothing certain for the others. Blood samples were obtained from each subject after informed consent for gene analysis was given. The patients had been analyzed for mutations in *SCN5A* by using specific primer pairs (Table S1), and no disease-related mutation was found. The control subjects were 480 genetically unrelated Japanese individuals who were selected at random without ECG records.

The research protocol was approved by the Ethics Review Committee of the Medical Research Institute, Tokyo Medical and Dental University and the Institutional Review Board of Samsung Medical Center.

Mutational Analysis

Genomic DNA extracted from the peripheral blood leukocytes of each individual was subjected to polymerase chain reaction (PCR) using primer pairs specific to *SCN3B* (Table S2). PCR products were analyzed for mutations by direct DNA sequencing using Big Dye Terminator version 3.1 and ABI3100 DNA analyzer (Applied Biosystems, Foster City, CA, USA). The proband patients carrying the Val110Ile mutation were analyzed for mutations in the other known BrS susceptibility genes, *CACNA1C*, *CACNB2*, *GPD1-L*, *KCNJ8*, *SCN1B*, *KCNE3*, *MOG1*, *HCN4*, *KCND3* and *KCNE5*, by sequencing of PCR products amplified with specific primer pairs (Table S1).

Alignment of Amino Acid Sequences

Amino acid sequences of human Navβ3 protein predicted from the nucleotide sequences (GenBank™ NM_018400) were aligned with those of chimpanzee (XM_522210), macaque (NM_001194283), mouse (NM_153522), rat (NM_139097), rabbit (ENSOCUP00000009050), bovine (NM_001046495), horse (ENSECAT00000025763), dog (XM_847682), elephant (ENSLAFT00000000307), opossum (XM_001379934), platypus (ENSOANT00000023925), chicken (XM_417884), *Xenopus* (NM_001011299), and zebrafish (NM_001080802).

Constructs for Nav1.5 and Navβ3

We obtained a cDNA fragment of human Navβ3 by reverse transcription-PCR from human adult heart cDNA. Mutant cDNA fragments of Navβ3 containing a T to C substitution in codon 10 (for Leu10Pro mutation) or a G to A substitution at codon 110 (for Val110Ile mutation) were created by the primer-mediated mutagenesis method using specific primers (Table S3). Wild-type (WT) or mutant cDNA fragments were cloned into pcDNA3.1-myc, His-B (myc-His-Navβ3) (Invitrogen, San Diego, CA, USA) and pIRES-CD8 (pIRES-CD8-Navβ3). The cDNA fragment of human *SCN5A* was a gift from Dr A.L. George (Vanderbilt University). A Flag-tagged Nav1.5 was constructed by inserting a Flag epitope (DYKDDDDK) into the extracellular linker 1 (L1) between S1 and S2 in the D1 domain after position aa154 in the Nav1.5 construct (L1-Flag-Nav1.5), as described previously.[18] All constructs were sequenced to ensure that no errors were introduced.

Immunofluorescence Microscopy

We seeded 4.0×10^4 tsA-201 cells, a derivative line of HEK cells, onto poly-D-Lysine 8-well culture slides (BD Biosciences, San Jose, CA, USA), and 24 h later, myc-His-Navβ3 (0.1 μg) alone, or L1-Flag-Nav1.5 (0.1 μg) plus myc-His-Navβ3 (0.1 μg) were added to the wells with Lipofectamine 2000 Reagent (Invitrogen) (0.2 or 0.4 μl, respectively). After 18 h, the cells were washed with phosphate-buffered saline (PBS), fixed in 4% paraformaldehyde for 15 min at room temperature and permeabilized by 0.15% Triton X-100 in PBS with 3% bovine serum for 20 min at room temperature. The cells were then incubated with the primary rabbit anti-Flag polyclonal antibody (Ab) (1:250, Sigma, CA, USA) and mouse anti-myc monoclonal Ab (1:200, Santa Cruz Biotechnology, Santa Cruz, CA, USA), and secondary Alexa Fluor 568 goat anti-rabbit IgG (1:500, Molecular Probes, Eugene, OR, USA) and Alexa Fluor 488 rabbit anti-mouse IgG (1:1,000, Molecular Probes), respectively, in PBS with 3% bovine serum. All cells were mounted on glass slides using Mowiol 4-88 Reagent (Calbiochem, Darmstadt, Germany), and images were collected and analyzed with an LSM510 laser-scanning microscope (Carl Zeiss Microscopy, Jena, Germany). To quantify the membrane expression of Nav1.5, fluorescence intensity of the total cell and the plasma membrane (peripheral, 2 μm) areas in the middle *xy* images of *z* series stack were measured, and the ratios of peripheral to total cell area fluorescence intensity (PTAFI) were calculated as described previously.[23] Analyses of labeled cells were performed using ImageJ software (NIH, MD, USA).[31]

Electrophysiological Studies

The tsA-201 cell line was used in the electrophysiological study, as described previously.[18] Cells transfected with pIRES-CD8 or pIRES-CD8-Navβ3 were briefly preincubated with Dynabeads M-450 CD8 (Dynal, Oslo, Norway) prior to the recordings. Sodium currents were recorded from the cells that were labeled with Dynabeads using the whole-cell patch clamp technique. Currents and cell capacitances were recorded using Axopatch 200B amplifier (Axon Instruments, CA, USA) and series resistance errors were reduced by 60–70% using elec-

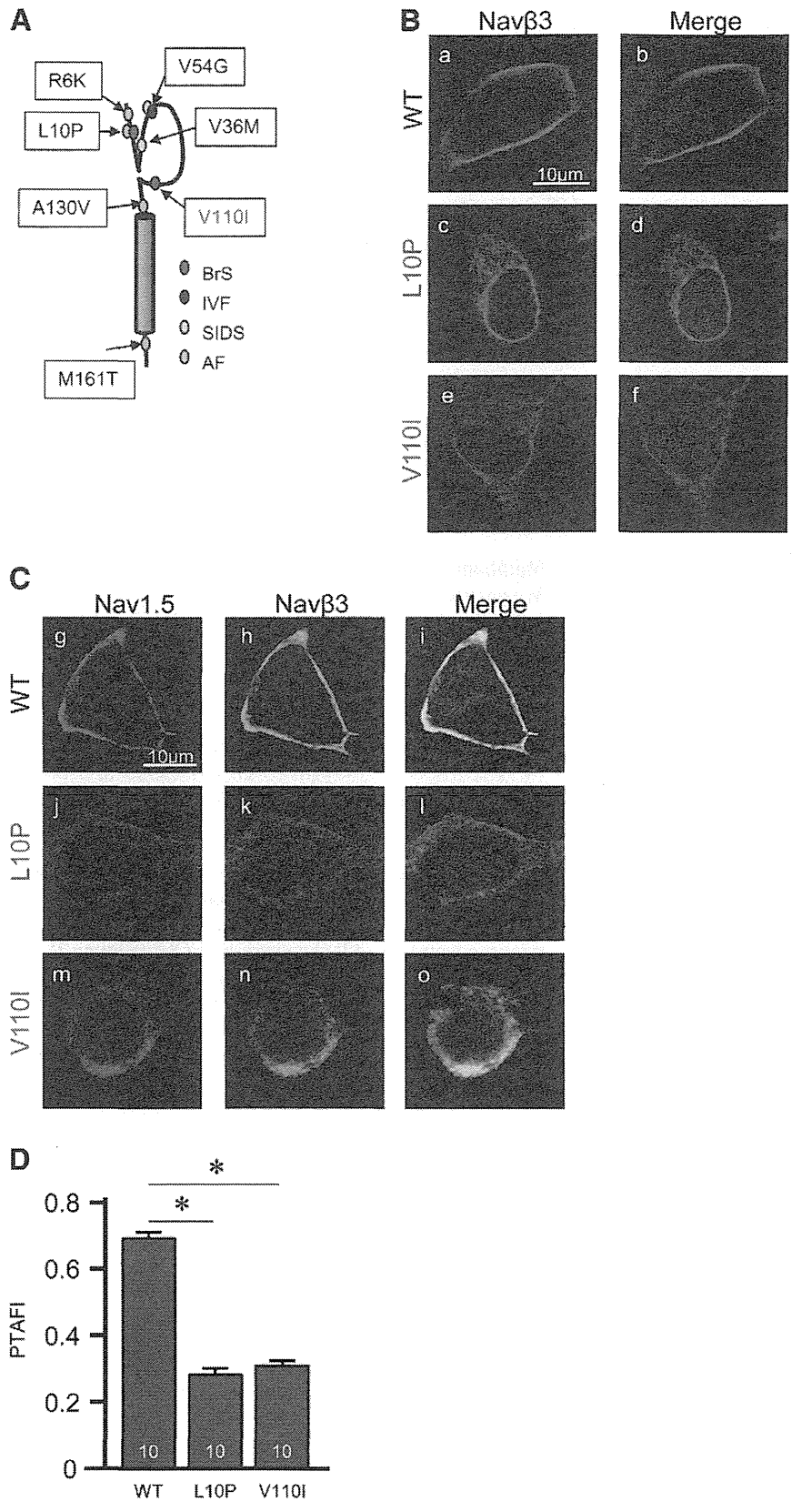

Figure 2. *SCN3B* mutations reported in arrhythmias and distribution of Nav1.5 and Navβ3 in transfected tsA-201 cells. (**A**) Schematic representation of Navβ3 mutations found in arrhythmias. *SCN3B* mutations in BrS (red), IVF (purple), SIDS (light green), and AF (light blue) are mapped on the Navβ3. Extracellular domain and transmembrane domain are indicated. The V110I mutation found in this study is indicated in red. (**B**,**C**) tsA-201 cells transfected with myc-His-Navβ3-WT (**a**,**b**), -L10P (**c**,**d**) or -V110I (**e**,**f**), and the combination of L1-Flag-Nav1.5 and myc-His-Navβ3-WT (**g**–**i**), -L10P (**j**–**l**), or -V110I (**m**–**o**). The cells were permeabilized by 0.15% Triton X-100 and stained with anti-myc Ab (Navβ3, green; **a**,**c**,**e**,**h**,**k**,**n**) and anti-Flag Ab (Nav1.5, red; **g**,**j**,**m**). Nuclei were stained with DAPI and merged images are shown in **b**,**d**,**f**,**i**,**l**, and **o**. Scale bar=10μm. (**D**) The ratio of peripheral to total cell area fluorescence intensity (PTAFI) of expressed L1-Flag-hNav1.5 in the transfected cells. Numbers of analyzed cells are indicated at the bottom of each bar. Data are expressed as mean± SEM. *P<0.001. AF, atrial fibrillation; BrS, Brugada syndrome; IVF, idiopathic ventricular fibrillation; SIDS, sudden infant death syndrome.

Table 2. Kinetics of I_{Na} in Transfected tsA-201 Cells

Transfected constructs	Peak I_{Na} (at −25 mV)		Activation			Inactivation			Recovery	
	pA/pF	n	$V_{1/2}$ (mV)	κ	n	$V_{1/2}$ (mV)	κ	n	Time required for e^{-1} fraction recovery (ms)	n
SCN5A without SCN3B	−59.83±11.36**	10	−35.23±1.83*	−7.49±0.29*	10	−78.66±1.59*	7.63±0.29*	10	10.29±0.81**	9
SCN5A+SCN3B-WT	−110.28±8.92	11	−43.22±2.11	−6.68±0.21	11	−82.40±1.96	6.83±0.15	11	6.06±1.10	9
SCN5A+SCN3B-L10P	−68.09±5.81**	13	−40.39±1.98	−6.51±0.17	13	−83.49±1.10	6.40±0.23	11	8.88±0.99**	10
SCN5A+SCN3B-V110I	−62.72±5.10**	15	−40.28±1.82	−6.35±0.12	15	−81.98±1.34	6.60±0.18	15	6.10±0.92	12
SCN5A+SCN3B-WT/L10P	−82.46±8.21*	13	−41.49±2.01	−6.27±0.19	13	−81.76±1.49	6.59±0.27	13	6.87±1.00	12
SCN5A+SCN3B-WT/V110I	−77.77±7.31**	13	−41.57±1.45	−6.16±0.26	13	−81.17±1.03	6.44±0.13	12	6.44±1.45	12

*P<0.05 vs. SCN5A+SCN3B-WT, **P<0.01 vs. SCN5A+SCN3B-WT.
I_{Na}, inward sodium current; WT, wild-type.

tronic compensation. Holding potentials were −120 mV and pipette resistance was 1.0–1.5MΩ. The bath solution contained 36 mmol/L NaCl, 109 mmol/L NMG, 4 mmol/L KCl, 1.8 mmol/L $CaCl_2$, 1 mmol/L $MgCl_2$, and 10 mmol/L HEPES, pH 7.35, while the pipette solution contained 10 mmol/L NaF, 110 mmol/L CsF, 20 mmol/L CsCl, 10 mmol/L EGTA, and 10 mmol/L HEPES, pH 7.35. All signals were acquired at 20–50 kHz (Digidata 1332, Axon Instruments) with a personal computer running Clampex 8 software (Axon Instruments) and filtered at 5 kHz with a 4-pole Bessel low-pass filter. Experiments were done at room temperature. Membrane currents were analyzed with Clampfit 8 software (Axon Instruments) and Sigmaplot (Systat Software, CA, USA). The current-voltage relationships were fit to the Boltzmann equation,

$$I=(V-V_{rev})\times G_{max}\times[1+\exp(V-V_{1/2})/\kappa]-1,$$

where I is the peak sodium current during the test pulse potential V. The parameters estimated by the fitting are V_{rev} (reversal potential), G_{max} (maximum conductance), and κ (slope factor). Steady-state availability was fit with the Boltzmann equation,

$$I/I_{max}=[1+\exp((V-V_{1/2})/\kappa)]-1,$$

where I_{max} is the maximum peak sodium current, to determine the membrane potential for $V_{1/2}$ (half-maximal inactivation) and κ (slope factor). The time course of inactivation was fit with a 2-exponential function,

$$I(t)/I_{max}=A0+A1\times\exp(-t/\tau_1)+A2\times\exp(-t/\tau_2),$$

where A and τ are amplitudes and time constants, respectively. I and t refer to current and time, respectively.

Co-Immunoprecipitation (co-IP) Assay

The tsA-201 cells were transiently transfected with a combination of L1-Flag-Nav1.5 (2 μg) and myc-His-Navβ3 (2 μg). Cellular extracts were prepared from the transfected cells and equal amount of extracted proteins were used for the co-IP assay using the Catch and Release version 2.0 reversible immunoprecipitation system, according to the manufacturer's instructions (Millipore, Milford, MA, USA), with rabbit anti-Flag polyclonal Ab (Sigma). Eluted samples were separated by SDS-PAGE, transferred to a nitrocellulose membrane, pre-incubated with 5% skimmed milk in PBS, and incubated with primary mouse anti-c-myc monoclonal Ab (1:100) followed by secondary rabbit anti-mouse (for monoclonal Ab) IgG HRP-conjugated Ab (1:1,000; Dako A/S, Glostrup, Denmark).

Statistical Analysis

Numerical data are expressed as mean±SEM. Statistical differences were analyzed using 1-way analysis of variance (ANOVA) followed by Dunnett's test. P<0.05 was considered to be statistically significant.

Results

Mutational Analysis of SCN3B

We analyzed 181 BrS patients, who were negative for *SCN5A* mutations, for sequence variations in *SCN3B* and found a synonymous and another non-synonymous variant in 1 and 3 patients, respectively. The synonymous variant, p.Asn113Asn (c.339C>T), was rare and was not considered to be a disease-causing mutation because no functional effect was deduced. On the other hand, the non-synonymous variant, p.Val110Ile (V110I, c.328G>A) (**Figure 1A**), was found in 3 unrelated Japanese patients; a 42-year-old male (BrS-O-1), a 33-year-old male (BrS-S-1), and a 51-year-old male (BrS-H-1) (**Table 1**). The V110I variant was predicted to affect an evolutionary conserved residue of Navβ3 (**Figure 1B**) and was not found in 960 control chromosomes. As summarized in **Table 1**, BrS-O-1 had experienced repetitive syncope, and showed spontaneous coved-type ST-elevation in ECG (**Figure 1C**). His daughter (BrS-O-2) was asymptomatic, but exhibited a BrS-like ECG pattern and carried the same mutation (**Table 1**, **Figure 1D**). BrS-S-1 was asymptomatic, showed saddleback-type ST-segment elevation, and pilsicainide administration converted the ST-segment elevation into the coved type. His father and sister had arrhythmia, although the details could not be evaluated (**Figure 1E**). BrS-H-1 had experienced syncope, and showed spontaneous coved-type ST-elevation in ECG, but the family history of arrhythmia was uncertain. These 3 proband patients were also analyzed for mutations in the other known disease genes for BrS (**Table S1**) and none had any mutation.

Cell Surface Expression of Nav1.5 in the Presence of Mutant Navβ3

Navβ3 modulates the function of the Nav1.5 channel, and several *SCN3B* mutations have been reported in association with arrhythmias, including BrS, IVF, SIDS, and AF (**Figure 2A**). Because the Leu10Pro (L10P) mutation was the only mutation previously reported in only 1 BrS patient, which resulted in the reduction of I_{Na} in transfected cells,[23] we investigated the functional alterations caused by the V110I mutation as compared with the L10P mutation. Membrane surface expression of Nav1.5 was examined in tsA-201 cells transfected with myc-His-Navβ3 alone or in combination with L1-Flag-Nav1.5. It was observed that Navβ3-WT was expressed on the cell

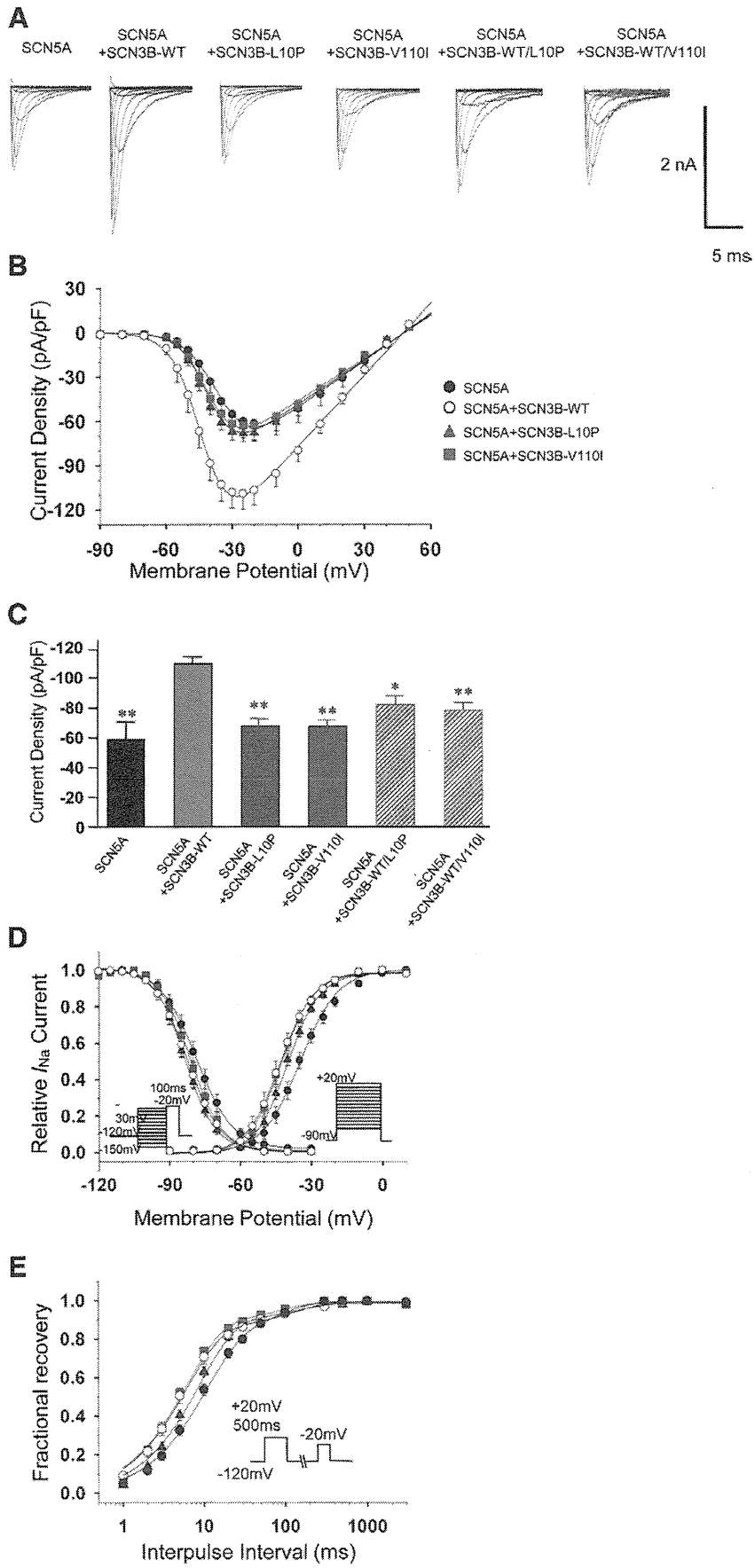

Figure 3. Electrophysiological profiles of sodium currents recorded from tsA-201 cells transiently expressing Nav1.5 and Navβ3. (**A**) Representative sodium currents recorded from tsA-201 cells cotransfected with pcDNA3.1-Nav1.5 and pIRES-CD8 or pIRES-CD8-Navβ3. The traces were recorded with a whole-cell configuration. (**B**) Current-voltage relationship for peak I_{Na}. (**C**) Sodium current density at –25 mV. Co-expression of Nav1.5 and Navβ3-WT increased the peak current densities by 83.9%, as compared with Nav1.5 alone, while co-expression of Nav1.5 with Navβ3-L10P or -V110I showed significantly smaller peak current densities than co-expression of Nav1.5 with Navβ3-WT by 37.5% and 42.5%, respectively (n=11 for WT, n=13 for L10P, n=15 for V110I). Co-expression of Nav1.5 and Navβ3-WT plus -L10P or -V110I also showed significantly smaller peak current densities than co-expression of Nav1.5 and Navβ3-WT by 25.2% or 29.4%, respectively (n=13 for WT/L10P, n=13 for WT/V110I). (**D**) Transfected cells of pcDNA3.1-Nav1.5 and pIRES-CD8-Navβ3-WT show a leftward shift in the voltage dependence of steady-state fast inactivation and activation, compared with transfected cells of pcDNA3.1-Nav1.5 and pIRES-CD8. Voltage dependences recorded from the transfected cells of pcDNA3.1-Nav1.5 in combination with pIRES-CD8-Navβ3-L10P, or -V110I were similar to that from the cells cotransfected with pcDNA3.1-Nav1.5 and pIRES-CD8-Navβ3-WT. (**E**) Transfected cells of pcDNA3.1-Nav1.5 and pIRES-CD8-Navβ3-WT show a leftward shift in the recovery from inactivation assessed by the double-pulse protocol, compared with transfected cells of pcDNA3.1-Nav1.5 and pIRES-CD8. Recovery from inactivation was nearly identical among Navβ3-WT, and -V110I, whereas L10P showed a significant rightward shift. The 2-pulse protocol is shown in the inset. WT, wild-type.

surface, whereas both Navβ3-L10P and Navβ3-V110I were retained in the cytoplasm (**Figures 2B-a–f**). In the cells co-transfected with Nav1.5 and myc-His-Navβ3, Nav1.5 was clearly expressed on the cell surface in the presence of Navβ3-WT (**Figures 2C-g–i**), but its cytoplasmic trafficking was disturbed by both Navβ3-L10P and Navβ3-V110I (**Figures 2C-j–o**). To express the trafficking defects quantitatively, we measured the fluorescence intensity of Nav1.5 in both the plasma membrane region and the entire cell area to obtain the ratios of PTAFI. As shown in **Figure 2D**, both the L10P and V110I mutation of *SCN3B* significantly reduced the cell surface expression of Nav1.5 by approximately 70%.

Altered Electrophysiological Characteristics of I_{Na} Caused by the *SCN3B* Mutations

Because the V110I mutation impaired the intracellular trafficking of Nav1.5, we investigated the potential effect of V110I mutation on Nav1.5 kinetics. Whole-cell patch clamp recordings were obtained from tsA-201 cells transiently transfected with pcDNA3.1-Nav1.5 in combination with pIRES-CD8, pIRES-CD8-Navβ3-WT, -L10P or -V110I (**Figure 3, Table 2**). It was found that the peak current densities of I_{Na} from the cells cotransfected with pcDNA3.1-Nav1.5 and pIRES-CD8-Navβ3-WT were significantly larger than that recorded from the cells cotransfected with pcDNA3.1-Nav1.5 and pIRES-CD8 by 83.9% (**Figures 3B,C, Table 2**). However, the peak current densities of I_{Na} recorded from the cells co-transfected with pcDNA3.1-Nav1.5 and pIRES-CD8-Navβ3-L10P or -V110I were significantly smaller than that recorded from the cells cotransfected with pcDNA3.1-Nav1.5 and pIRES-CD8-Navβ3-WT by 37.5% or 42.5%, respectively (**Figures 3B,C, Table 2**).

It also was observed that pIRES-CD8-Navβ3-WT shifted the voltage dependence of activation and inactivation to more negative potentials compared with pIRES-CD8, and neither pIRES-CD8-Navβ3-L10P nor -V110I caused any significant changes in the activation and inactivation kinetics of I_{Na} compared with pIRES-CD8-Navβ3-WT (**Figure 3D, Table 2**). In accordance with the previous report,[23] pIRES-CD8-Navβ3-L10P caused a rightward shift in the time course of recovery from inactivation, whereas pIRES-CD8-Navβ3-V110I did not show any significant changes (**Figure 3E, Table 2**). To analyze the functional impact of mutant Navβ3 in the heterozygous state, the sodium current was recorded from cells expressing Nav1.5 in combination with WT and mutant Navβ3. It was demonstrated that the peak current densities of I_{Na} recorded from the pcDNA3.1-Nav1.5-transected cells with pIRES-CD8-Navβ3-WT+L10P or -WT+V110I were significantly smaller than that from the transfected cells with pIRES-CD8-Navβ3-WT by 25.2% or 29.4%, respectively (**Table 2**). These data indicated that neither mutation exerted a dominant negative effect on the function of normal Navβ3.

Binding Between Nav1.5 and Navβ3

Because Navβ3 non-covalently interacts with Nav1.5, we investigated whether the V110I mutation would change the interaction, but there were no significant differences among Navβ3-WT, -L10P and -V110I in binding Nav1.5 (**Figure 4**), indicating that the altered sodium channel function was not caused by loss of binding between Nav1.5 and Navβ3.

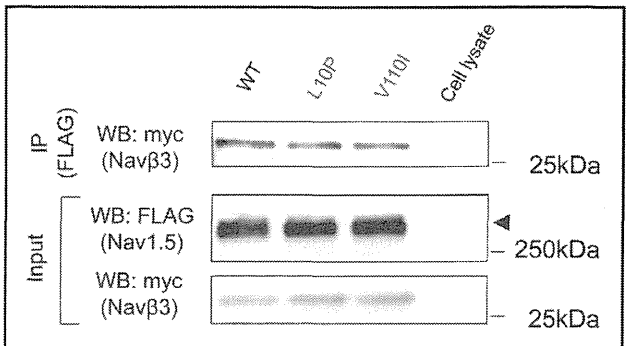

Figure 4. Binding assay between Navβ3 and Nav1.5. The tsA-201 cells were cotransfected with Flag-tagged Nav1.5 (L1-Flag-Nav1.5) and myc-tagged Navβ3 (myc-His-Navβ3) of WT, L10P or V110I. Cell lysates were prepared and subjected to western blot analyses after immunoprecipitation with the anti-Flag polyclonal Ig. (**Upper**) Amounts of myc-tagged Navβ3 after immunoprecipitation detected by anti-myc antibody. (**Lower**) Amounts of input proteins, Flag-tagged Nav1.5 and myc-tagged Navβ3, detected by anti-Flag and anti-myc antibodies, respectively. Positions of size markers are indicated at the right. WT, wild-type.

Discussion

Arrhythmias can be caused by mutations in the genes for cardiac ion channels producing action potentials. In BrS, the inward sodium current (I_{Na}) is more frequently affected than the other currents such as calcium and potassium.[32] To date, more than 300 disease-causing *SCN5A* mutations have been reported, and have been detected in 11–28% of BrS patients.[11,32] On the other hand, the prevalence of BrS-causing mutations in the genes for modifier proteins of Nav1.5, including GPD1-L, Navβ1, Navβ3 and MOG1, is relatively low.[23,24,32] In the present study, we identified a novel *SCN3B* mutation, V110I, in 3 Japanese BrS patients. It affected the evolutionary conserved residue of Navβ3, not found in the control subjects, decreased the cell surface expression of Nav1.5, and impaired I_{Na} function. These observations strongly suggested that the *SCN3B* mutation was a BrS-causing mutation. It is noteworthy that, among these 3 patients, 2 had family histories of arrhythmia and/or sudden cardiac death, while the family history was uncertain in the other patient, indicating that the *SCN3B* mutation was rare but could be found in a considerable proportion of *SCN5A*-negative BrS, especially familial cases; 2 in 19 (10.5%) familial cases and 1 in 159 (0.6%) sporadic cases. Although there were no traceable genetic relations among the proband patients carrying the same mutation, the V110I mutation might be a founder mutation. Further investigation of the *SCN3B* mutation in a large cohort of familial BrS cases is required to assess the ancestral origin of mutation.

The cell surface expression of Nav1.5 was significantly reduced in the presence of Navβ3-L10P or-V110I in transfected cells. Although the cytoplasmic trafficking defect of Nav1.5 is well known to be an underlying mechanism for cardiac channelopathies, including BrS,[20,33] involvement of modifier proteins in the cell surface expression of Nav1.5 is poorly understood.[34] A pore-forming subunit of the voltage-gated sodium channel in the sensory nervous and atrial myocardium, Nav1.8, is highly homologous to Nav1.5.[35] It was reported that an endoplasmic reticulum (ER) retention sequence, RRR, in the cytoplasmic loop I of Nav1.8 caused retention of Nav1.8 on the ER, and masking of the retaining signal by Navβ3 released Nav1.8 for trafficking to the cell surface.[36] Because the RRR sequence is conserved in the cytoplasmic loop I of Nav1.5, Navβ3 might alter Nav1.5 trafficking by masking its ER reten-

tion signal. However, immunofluorescence studies demonstrated cytoplasmic colocalization of Nav1.5 and Navβ3, even in the presence of *SCN3B* mutations. This, in turn, implied that the trafficking defect of Nav1.5 was not caused by impaired formation of the sodium channel complex but by retention of mutant Navβ3 in the ER.

To date, 5 different β-subunits of the sodium channel have been identified.[25,34] In cardiomyocytes, Navβ1 and Navβ3 are preferentially expressed and modulate the function of Nav1.5 through non-covalent binding.[25] the structure of the β-subunits is relatively simple; forming with an Ig loop at the extracellular N-terminal region, 1 transmembrane domain, and a small intracellular C-terminal domain. In this study, both the L10P and V110I mutations affected the peak current of I_{Na} in transfected cells via an affect on the trafficking of Nav1.5 to the cell surface. The binding of Nav1.5 and Navβ3, however, was not affected by the *SCN3B* mutations, suggesting that the Ig loop might not be involved in the binding to Nav1.5. On the other hand, these mutations showed different effects on the recovery from inactivation, indicating the possibility that the modulation of Nav1.5 function by Navβ3 might be controlled at multiple steps. It is interesting to note that the L10P mutation is also reported in AF.[30] The underlying mechanism of AF is a reentrant circuit in atrial tissues, where electrical conduction is delayed.[4,37] In patients with inherited AF who carried the *SCN5A* mutation, the delayed conductance is predicted to be induced by a slower upstroke of the action potential because of the loss-of-function mutation in *SCN5A*.[4] As shown in **Figure 3E**, slower recovery from inactivation associated with the L10P mutation might partly contribute to the further delayed upstroke of the action potential by decreasing the fraction of channels enrolling in the subsequent depolarization. The difference in inactivation recovery might be related to the differences in arrhythmic phenotypes.

We revealed that the L10P mutation decreased peak sodium current density by 37.5%. On the other hand, Hu et al reported that the L10P mutation decreased the peak current density by 80%, and approximately 40% of the transfectants did not produce the current,[23] and Olsen et al showed that the L10P decreased the peak currents by approximately 50%.[30] The reasons for these functional differences might be related to the different experimental conditions, including cell lines, the ratio of vectors, the presence of Navβ1, and the chemical composition of the bath solution. These differences would complicate the understanding and comparing of functional alterations caused by the mutations.

In summary, we identified a *SCN3B* V110I mutation in 3 unrelated Japanese patients with BrS that impaired intracellular trafficking and affected the electrophysiological function of Nav1.5, a hallmark of BrS. This is the first replicating report demonstrating a *SCN3B* mutation as a disease gene for BrS.

Acknowledgments

This work was supported in part by Grant-in-Aids for Scientific Research from the Ministry of Education, Culture, Sports, Science and Technology, Japan; a Health and Labor Sciences Research Grant from the Ministry of Health, Labour and Welfare, Japan; grants for Basic Scientific Cooperation Program between Japan and Korea from the Japan Society for the Promotion of Science and the National Research Foundation, Korea, follow-up grants from the Tokyo Medical and Dental University, and Joint Usage/Research Program of Medical Research Institute Tokyo Medical and Dental University.

Disclosures

Conflict of Interest: None declared.

References

1. Brugada P, Brugada J. Right bundle branch block, persistent ST segment elevation and sudden cardiac death: A distinct clinical and electrocardiographic syndrome: A multicenter report. *J Am Coll Cardiol* 1992; **20:** 1391–1396.
2. Chen Q, Kirsch GE, Zhang D, Brugada R, Brugada J, Brugada P, et al. Genetic basis and molecular mechanism for idiopathic ventricular fibrillation. *Nature* 1998; **392:** 293–296.
3. Berne P, Brugada J. Brugada syndrome 2012. *Circ J* 2012; **76:** 1563–1571.
4. Amin AS, Tan HL, Wilde AA. Cardiac ion channels in health and disease. *Heart Rhythm* 2010; **7:** 117–126.
5. Schulze-Bahr E, Eckardt L, Breithardt G, Seidl K, Wichter T, Wolpert C, et al. Sodium channel gene (SCN5A) mutations in 44 index patients with Brugada syndrome: Different incidences in familial and sporadic disease. *Hum Mutat* 2003; **21:** 651–652.
6. Medeiros-Domingo A, Tan BH, Crotti L, Tester DJ, Eckhardt L, Cuoretti A, et al. Gain-of-function mutation S422L in the KCNJ8-encoded cardiac K(ATP) channel Kir6.1 as a pathogenic substrate for J-wave syndromes. *Heart Rhythm* 2010; **7:** 1466–1471.
7. Ueda K, Hirano Y, Higashiuesato Y, Aizawa Y, Hayashi T, Inagaki N, et al. Role of HCN4 channel in preventing ventricular arrhythmia. *J Hum Genet* 2009; **54:** 115–121.
8. Kattygnarath D, Maugenre S, Neyroud N, Balse E, Ichai C, Denjoy I, et al. MOG1: A new susceptibility gene for Brugada syndrome. *Circ Cardiovasc Genet* 2011; **4:** 261–268.
9. Burashnikov E, Pfeiffer R, Barajas-Martinez H, Delpon E, Hu D, Desai M, et al. Mutations in the cardiac L-type calcium channel associated with inherited J-wave syndromes and sudden cardiac death. *Heart Rhythm* 2010; **7:** 1872–1882.
10. Giudicessi JR, Ye D, Tester DJ, Crotti L, Mugione A, Nesterenko VV, et al. Transient outward current (I(to)) gain-of-function mutations in the KCND3-encoded Kv4.3 potassium channel and Brugada syndrome. *Heart Rhythm* 2011; **8:** 1024–1032.
11. Kapplinger JD, Tester DJ, Alders M, Benito B, Berthet M, Brugada J, et al. An international compendium of mutations in the SCN5A-encoded cardiac sodium channel in patients referred for Brugada syndrome genetic testing. *Heart Rhythm* 2010; **7:** 33–46.
12. Wilde AA, Brugada R. Phenotypical manifestations of mutations in the genes encoding subunits of the cardiac sodium channel. *Circ Res* 2011; **108:** 884–897.
13. Hermida JS, Lemoine JL, Aoun FB, Jarry G, Rey JL, Quiret JC. Prevalence of the brugada syndrome in an apparently healthy population. *Am J Cardiol* 2000; **86:** 91–94.
14. Antzelevitch C, Brugada P, Borggrefe M, Brugada J, Brugada R, Corrado D, et al. Brugada syndrome: Report of the second consensus conference: Endorsed by the Heart Rhythm Society and the European Heart Rhythm Association. *Circulation* 2005; **111:** 659–670.
15. Miyasaka Y, Tsuji H, Yamada K, Tokunaga S, Saito D, Imuro Y, et al. Prevalence and mortality of the Brugada-type electrocardiogram in one city in Japan. *J Am Coll Cardiol* 2001; **38:** 771–774.
16. Abriel H. Cardiac sodium channel Na(v)1.5 and interacting proteins: Physiology and pathophysiology. *J Mol Cell Cardiol* 2010; **48:** 2–11.
17. Ashino S, Watanabe I, Kofune M, Nagashima K, Ohkubo K, Okumura Y, et al. Effects of quinidine on the action potential duration restitution property in the right ventricular outflow tract in patients with brugada syndrome. *Circ J* 2011; **75:** 2080–2086.
18. Makita N, Behr E, Shimizu W, Horie M, Sunami A, Crotti L, et al. The E1784K mutation in SCN5A is associated with mixed clinical phenotype of type 3 long QT syndrome. *J Clin Invest* 2008; **118:** 2219–2229.
19. Watanabe H, Nogami A, Ohkubo K, Kawata H, Hayashi Y, Ishikawa T, et al. Electrocardiographic characteristics and SCN5A mutations in idiopathic ventricular fibrillation associated with early repolarization. *Circ Arrhythm Electrophysiol* 2011; **4:** 874–881.
20. Ackerman MJ, Siu BL, Sturner WQ, Tester DJ, Valdivia CR, Makielski JC, et al. Postmortem molecular analysis of SCN5A defects in sudden infant death syndrome. *JAMA* 2001; **286:** 2264–2269.
21. Makiyama T, Akao M, Shizuta S, Doi T, Nishiyama K, Oka Y, et al. A novel SCN5A gain-of-function mutation M1875T associated with familial atrial fibrillation. *J Am Coll Cardiol* 2008; **52:** 1326–1334.
22. Watanabe H, Koopmann TT, Le Scouarnec S, Yang T, Ingram CR, Schott JJ, et al. Sodium channel beta1 subunit mutations associated with Brugada syndrome and cardiac conduction disease in humans. *J Clin Invest* 2008; **118:** 2260–2268.
23. Hu D, Barajas-Martinez H, Burashnikov E, Springer M, Wu Y, Varro A, et al. A mutation in the beta 3 subunit of the cardiac sodium channel associated with Brugada ECG phenotype. *Circ Cardiovasc Genet*

2009; **2:** 270–278.
24. London B, Michalec M, Mehdi H, Zhu X, Kerchner L, Sanyal S, et al. Mutation in glycerol-3-phosphate dehydrogenase 1 like gene (GPD1-L) decreases cardiac Na^+ current and causes inherited arrhythmias. *Circulation* 2007; **116:** 2260–2268.
25. Brackenbury WJ, Isom LL. Na channel beta subunits: Overachievers of the ion channel family. *Front Pharmacol* 2011; **2:** 53.
26. Fahmi AI, Patel M, Stevens EB, Fowden AL, John JE 3rd, Lee K, et al. The sodium channel beta-subunit SCN3b modulates the kinetics of SCN5a and is expressed heterogeneously in sheep heart. *J Physiol* 2001; **537:** 693–700.
27. Valdivia CR, Medeiros-Domingo A, Ye B, Shen WK, Algiers TJ, Ackerman MJ, et al. Loss-of-function mutation of the SCN3B-encoded sodium channel {beta}3 subunit associated with a case of idiopathic ventricular fibrillation. *Cardiovasc Res* 2010; **86:** 392–400.
28. Tan BH, Pundi KN, Van Norstrand DW, Valdivia CR, Tester DJ, Medeiros-Domingo A, et al. Sudden infant death syndrome-associated mutations in the sodium channel beta subunits. *Heart Rhythm* 2010; **7:** 771–778.
29. Wang P, Yang Q, Wu X, Yang Y, Shi L, Wang C, et al. Functional dominant-negative mutation of sodium channel subunit gene SCN3B associated with atrial fibrillation in a Chinese GeneID population. *Biochem Biophys Res Commun* 2010; **398:** 98–104.
30. Olesen MS, Jespersen T, Nielsen JB, Liang B, Moller DV, Hedley P, et al. Mutations in sodium channel beta-subunit SCN3B are associated with early-onset lone atrial fibrillation. *Cardiovasc Res* 2011; **89:** 786–793.
31. Abramoff M, Magelhaes P, Ram S. Processing with ImageJ. *Biophoton Int* 2004; **11:** 36–42.
32. Hedley PL, Jorgensen P, Schlamowitz S, Moolman-Smook J, Kanters JK, Corfield VA, et al. The genetic basis of Brugada syndrome: A mutation update. *Hum Mutat* 2009; **30:** 1256–1266.
33. Watanabe H, Darbar D, Kaiser DW, Jiramongkolchai K, Chopra S, Donahue BS, et al. Mutations in sodium channel beta1- and beta2-subunits associated with atrial fibrillation. *Circ Arrhythm Electrophysiol* 2009; **2:** 268–275.
34. Rook MB, Evers MM, Vos MA, Bierhuizen MF. Biology of cardiac sodium channel Nav1.5 expression. *Cardiovasc Res* 2012; **93:** 12–23.
35. Facer P, Punjabi PP, Abrari A, Kaba RA, Severs NJ, Chambers J, et al. Localisation of SCN10A gene product Na(v)1.8 and novel pain-related ion channels in human heart. *Int Heart J* 2011; **52:** 146–152.
36. Zhang ZN, Li Q, Liu C, Wang HB, Wang Q, Bao L. The voltage-gated Na+ channel Nav1.8 contains an ER-retention/retrieval signal antagonized by the beta3 subunit. *J Cell Sci* 2008; **121:** 3243–3252.
37. Burstein B, Nattel S. Atrial fibrosis: Mechanisms and clinical relevance in atrial fibrillation. *J Am Coll Cardiol* 2008; **51:** 802–809.

Supplementary Files

Supplementary File 1

Table S1. Nucleotide Sequences of Primers Used for Mutational Analysis of the Other Known Brugada Syndrome Genes

Table S2. Nucleotide Sequences of Primers Used in the Mutational Analysis of *SCN3B*

Table S3. Nucleotide Sequences of Primers Used in the Construction of Navβ3 Constructs

Please find supplementary file(s);
http://dx.doi.org/10.1253/circj.CJ-12-0995

J Med Dent Sci 2013; 60: 17–22

Original Article

The generation of induced pluripotent stem cells from a patient with *KCNH2* G603D, without LQT2 disease associated symptom

Shinichiro Okata[1,2], Shinsuke Yuasa[1], Teiichi Yamane[3], Tetsushi Furukawa[2] and Keiichi Fukuda[1]

1) Department of Cardiology, Keio University School of Medicine, Japan.
2) Department of Bio-informational Pharmacology, Medical Research Institute, Tokyo Medical and Dental University, Japan.
3) Department of Cardiology, The Jikei University School of Medicine, Tokyo, Japan

The long QT syndrome type 2 (LQT2) is inheritable life threatening arrhythmic disorder and one of the most common genetic variants in long QT syndrome. There are some indications for treatment of the patients with LQT2 but it is impossible to completely prevent fatal arrhythmia. To develop novel therapy for the patients with LQT2, it has been desired to generate disease-specific and patient-specific disease model. Human induced pluripotent stem (iPS) cells are somatic cell-derived pluripotent stem cells with infinite proliferation ability and multipotency. Patient-specific iPS cells can be derived from patient somatic cells, have all genomic information encoded in patient's genome including mutation and all SNPs, and can be ideal disease models of the patients. To generate disease model for LQT2 by iPS cells, we should firstly generate iPS cells from the patient with LQT2 and confirm the genomic mutation in iPS cells. In this study, we showed the successful generation of iPS cells from a patient with *KCNH2* G603D mutation. The patient specific iPS cells properly expressed stem cell markers, such as NANOG and OCT3/4. We also confirmed that the *KCNH2* G603D (G1808A) mutation was taken over in patient specific iPS cells. These patient-specific iPS cells may contribute to the future analysis for disease pathogenesis and drug innovation.

Key words: iPS cell, Long QT syndrome, Disease modeling

Corresponding Author: Shinsuke Yuasa, M.D, Ph.D.
Assistant Professor, Department of Cardiology, Keio University School of Medicine, 35 Shinanomachi Shinjuku-ku, Tokyo, 160-8582, Japan.
Tel: +81-3-5363-3373 Fax: +81-3-5363-3875
E-mail: yuasa@a8.keio.jp
Received September 27 : Accepted November 16, 2012

Introduction

The generation of induced pluripotent stem (iPS) cell is firstly reported in 2006 with great surprise[1]. Human iPS cells are similar to human embryonic stem (ES) cells in terms of proliferation and differentiation ability, and can be generated from adult somatic cells[2,3]. Now we can easily generate iPS cells from patient's somatic cells and those iPS cells have all genomic information of the patient genome[4]. Many human diseases are caused by genomic mutation. Disease modeling using human iPS cells is newly emerged research field to analyze genetic human diseases[7]. Actually, there are many fatal genetic diseases without effective therapy. To develop newly effective therapies for those diseases, first of all we have to generate disease models. In the past, there had been solely animal models of human genetic disease, such as specific gene knockout mice, transgenic mice and autochthonous diseased animals. Although those models gave us many valuable information regarding to the mechanisms of human genetic diseases, most crucial problem is that those models are not human. So it is often difficult to model human diseases using experimental animals. In another important point of view, among humans, each individual shows highly rich in genomic diversity in terms of racial differences and single nucleotide polymorphisms (SNPs). So it has been highly expected to generate not only disease-specific models, but also disease-specific and patient-specific disease models. To

generate patient-specific disease models, now we can use iPS cells.

Long QT syndrome is one of the most common fatal cardiac arrhythmic disorders[8]. Recent molecular and electrophysiological examination established the fundamental disease concepts. But there is no definitive therapy invented so far. Here again, one of the most important points in drug discovery is to generate excellent disease models. Current experimental models for arrhythmic disorders mostly depend on animal model and heterologous expression system in human non-cardiomyocytes or non-human cardiomyocytes. The long QT syndrome type 2 (LQT2) is one of the most common genetic variants in long QT syndrome, and accounts for approximately 40% of genotyped patients[9]. LQT2 is caused by mutation of a potassium channel gene, *hERG* (human ether-a-go-go related gene), now referred to *KCNH2*. To generate the physiological cardiac action potential in human cardiomyocytes, in addition to inward sodium and calcium currents, several potassium currents are notably involved. The inward-rectifier background current (I_{K1}), the rapidly activating and inactivating transient outward current (I_{to}), and the ultrarapid (I_{Kur}), rapid (I_{Kr}), and slow (I_{Ks}) components of delayed rectifier currents. Those potassium currents have pivotal roles in electrophysiological homeostasis in human cardiomyocytes and the mutations in potassium current genes result in several human arrhythmic disorders. *KCNH2* encodes the a-subunit of the I_{Kr} channel, and membrane depolarization induced by strong inward currents produces a sequence of conformation changes within the channel that allows permeation of potassium ions. As a clinical phenotype, LQT2 is likely to result in cardiac events during exercise or emotional stress in more than half cases and during rest or sleep in some cases. More specifically, an auditory stimulus (telephone, alarm clock, ambulance siren, etc) can be a specific trigger in LQT2[10]. β-blocker use significantly reduces the risk of cardiac arrhythmic events in LQT2. And maintenance of the extracellular potassium concentration by long-term oral potassium supplementation is also reported to be effective because it shortens the QT interval in LQT2 patients. Besides those therapies, we cannot fully prevent sudden cardiac death in LQT2 patients. So we have to carry on the drug development for LQT2 by using LQT2 disease model.

In this study we showed the generation of iPS cells from a patient with *KCNH2* G603D mutation. These patient-specific iPS cells may contribute to future analysis for disease pathogenesis and drug innovation.

Materials and Methods

Patient consent

All subjects provided informed consent for blood testing for genetic abnormalities associated with hereditary long QT syndrome. The isolation and use of patient somatic cells was approved by the Ethics Committee of Keio University (approval no. 20-92-5) and the Ethics Committee of Tokyo Medical and Dental University (approval no. 2009-27), and was performed only after the patient and the parent had provided written informed consent.

Generation of human iPS cell

Human iPS cells were established from T lymphocytes as described previously[11,12]. Briefly, peripheral blood mononuclear cells (PBMCs) were separated by the centrifugation of heparinized whole blood sample obtained, using a Ficoll-Paque PREMIUM (GE Healthcae) gradient. The mononuclear cells were seeded on the anti-human CD3 antibody (BD Pharmingen)-coated 6-well plates in 2 mL GT-T502 (KOJIN BIO) medium per well, and incubated for 5 to 7 days until the activated T cells reached 80% to 90% confluent. Activated PBMCs were collected and transferred at 1.5×10^6 cells per well to a fresh anti-CD3 antibody coated 6-well plate, and incubated for an additional 24 hours. Then, the solution which contained sendai virus vectors individually carrying each of *OCT3/4*, *SOX2*, *KLF4*, and *c-MYC* were added at 10 MOI. After 24 hours of infection, the medium was changed to fresh GT-T502 medium, and the cells were collected and split at 5×10^4 cells into 10 cm-plates pre-seeded with mouse embryonic fibroblasts (MEFs) at more 24 hours after infection. After an additional 24 hours of incubation, the medium was changed to human iPS cell medium supplemented with 4 ng/mL of bFGF. The cells were cultured for another 20 days. On day 25, ES cell-like colonies were dissociated mechanically and transferred to a 24 well plate on the MEF feeder cells.

iPS cell culture

Human iPS cells were maintained on irradiated MEF feeder cells in human iPS cell culture medium, consisting of 80% DMEM/F12 (Sigma-Aldrich), 20% KO Serum Replacement (Invitrogen), 4 ng/mL basic fibroblast growth factor (bFGF; WAKO), 2 mmol/L L-glutamine (Invitrogen), 0.1 mmol/L non-essential amino acids (Sigma-Aldrich), 0.1 mmol/L 2-mercaptoethanol, 100 U/mL penicillin, and 100 μg/mL streptomycin

(Invitrogen). The human iPS cell medium was changed every 2 days and the cells were passaged using 1 mg/mL collagenase IV (Invitrogen) every 5-7 days. 293FT cells were cultured in DMEM supplemented with 10% FBS (Nichirei Bioscience), 1 × 10^{-4} M non-essential amino acids (NEAA; Sigma-Aldrich), 2 mmol/L L-glutamine (Invitrogen), 100 U/mL penicillin, and 100 μg/mL streptomycin (Invitrogen).

Immunocytochemistry

Immunostaining was used to analyze the expression of pluripotency markers. Cells were placed on a 35 mm glass-bottomed dish (IWAKI) before being fixed with 4% paraformaldehyde for 30 min at 4℃. The cells were then rinsed three times with phosphate-buffered saline (PBS) and permeabilized with 0.2% Triton-X 100 in PBS. The cells were then washed and blocked with Immunoblock (DS Pharma) three times for 5 min each time. Samples were incubated overnight at 4℃ with each of the primary antibodies: anti-NANOG (1:200 dilution; ab21624; Abcam), anti-OCT3/4 (1:100 dilution; sc-5279; Santa Cruz). Following incubation with primary antibodies, samples were incubated at room temperature for 1 h with the following secondary antibodies: Alexa Fluor 488 chicken anti-mouse IgG (1:200 dilution; A21200; Invitrogen), and Alexa Fluor 594 goat anti-rabbit IgG (1:200 dilution; A11037; Invitrogen). After cells had been washed by PBS, samples were mounted using Vectashield Hard Set Mounting Medium with 4′,6′-diamidino-2-phenylindole (DAPI) (Vector Laboratories) for nuclear staining. Images were obtained using a × 10 objective lens (NA = 0.45) on a fluorescence microscope (BZ-9000; Keyence).

Genome sequencing

DNA sequencing was used to confirm the presence of the LQT2 mutation in patient-derived iPSCs. Genomic DNA was isolated using a Gentra Puregene Cell Kit (Qiagen) and the region encoding *KCNH2*, including the mutation, was amplified using polymerase chain reaction (PCR) with the following primer set: 5′-TAGCCTGCATCTGGTACGC-3′ (forward) and 5′-GCCCGCCCCTGGGCACACTCA-3′ (reverse). The PCR product (277 bp) was electrophoresed on a 1% agarose gel and purified using a Wizard SV Gel and PCR Clean-Up System (Promega). The purified PCR product was sequenced with original primers.

Results

Novel *KCNH2* mutation

A 10-year-old man was given surgery for funnel chest, without any symptoms. Before operation, routine surface electrocardiogram (ECG) was recorded (Figure 1A). At that time, QT interval prolongation at ECG was firstly pointed out. The patient had no history of previous syncopal episode, palpitation or other cardiac symptoms. But his mother showed repetitive syncopal episodes at rest, triggered by sudden loud noises such as alarm clock and telephone call. Exercise testing shortened the QT interval and epinephrine challenge induced the QT interval prolongation and the form of polymorphic ventricular tachycardia called torsades de pointes. She underwent the genetic test which showed the novel *KCNH2* G603D (G1808A) mutation. Therefore he also underwent the genotype analysis which also showed the novel *KCNH2* G603D (G1808A) mutation (Figure 1B).

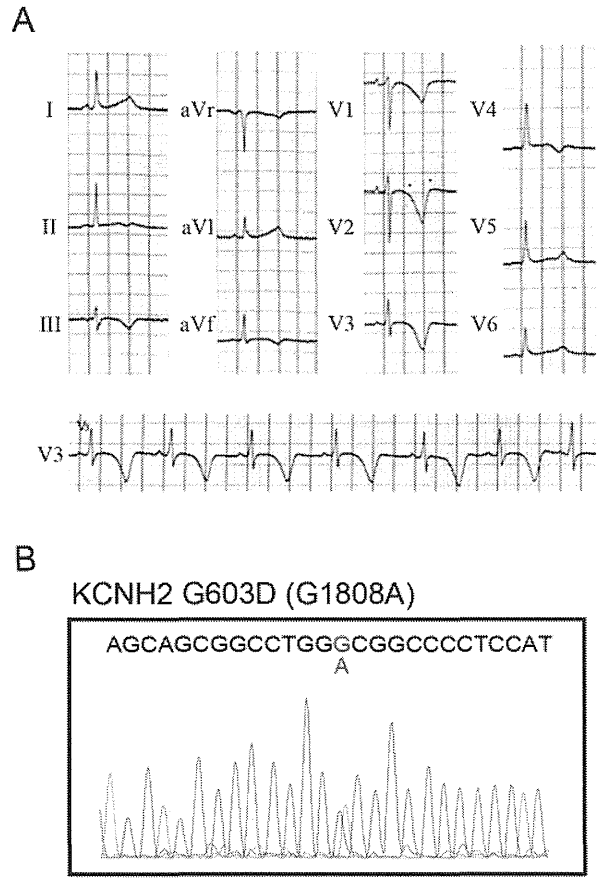

Figure 1. Novel *KCNH2* mutation in the patient.
A. Electrocardiogram from the patient during sinus rhythm. **B.** Sequence analysis of genomic *KCNH2* in the patient. The novel *KCNH2* G603D (G1808A) mutation.

iPS cell generation from a patient with *KCNH2* mutation

To generate iPS cells, we used peripheral blood cells as donor somatic cells from the patient. Separated peripheral mononuclear cells were stimulated by CD3 antibody and IL-2 to activate T lymphocytes. And activated T lymphocytes were reprogrammed by using Sendai virus carrying *SOX2*, *OCT3/4* (also known as *POU5F1*), *KLF4*, and *MYC*. Several clones were generated, expanded and stored. All iPS cell lines showed typical iPS cell morphology and expressed human pluripotency markers (Fig. 2a and b). These iPS cells were moved to petri-dishes and formed embryoid bodies with spontaneous beating, which indicated that these patient-specific iPS cells properly differentiated into beating cardiomyocytes *in vitro*.

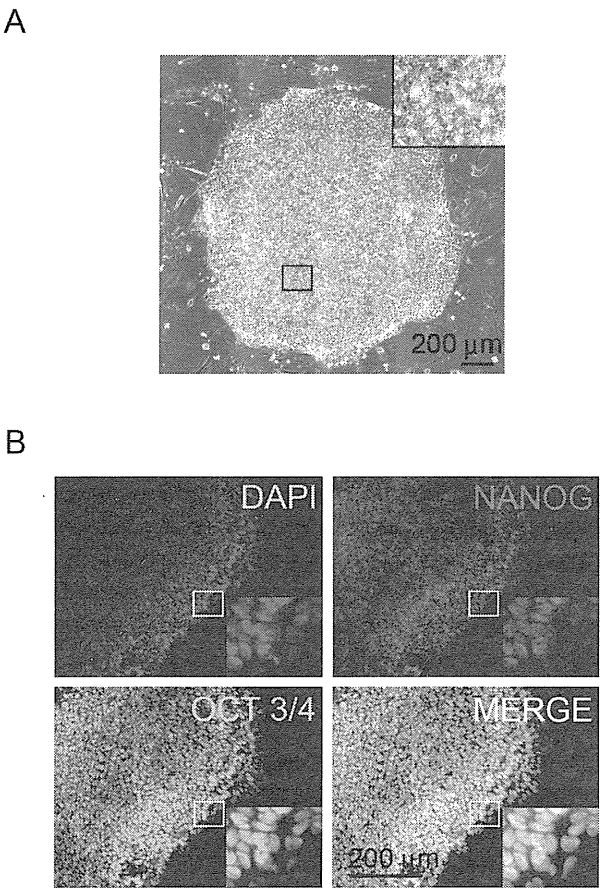

Figure 2. Generation of iPS cells from the patient with *KCNH2* G603D (G1808A) mutation.
A. Representative phase-contrast image of patient-specific iPS cell colony. Black box in figure is shown at a higher magnification in the inset. **B.** Immunofluorescence staining for stem cell markers (OCT3/4, NANOG and DAPI) in the patient-specific iPS cell colony. White boxes in each figure are shown at a higher magnification in the inset.

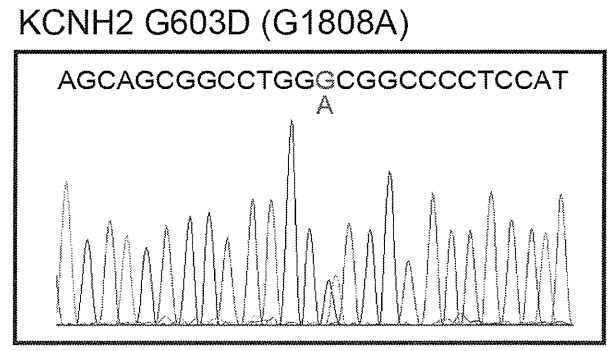

Figure 3. Novel *KCNH2* mutation in the patient-specific iPS cell colony.
Sequence analysis of genomic *KCNH2* in the patient-specific iPS cell colony. The novel *KCNH2* G603D (G1808A) mutation.

KCNH2 mutation in iPS cells derived from a patient with *KCNH2* mutation

To confirm that the generated iPS cells have a same mutation as the patient has, the genotype analysis was performed. It revealed the *KCNH2* G603D (G1808A) mutation was taken over (Figure 3).

Discussion

In the present study, we successfully generated iPS cells from a patient with the *KCNH2* G603D mutation who didn't exhibit any symptoms but showed prolonged QT interval at ECG. This patient is still young and may exhibit the cardiac symptom in the future. In real clinical setting, it is very important to know whether patients with genetic mutation will develop severe diseases or not. If we can predict the severity in the future disease manifestation, we can easily determine to do those patients, e.g., intensive care, exercise limitation, no medication and so on. So it is valuable to establish patient-specific disease model and develop the systems to evaluate the characteristics of patient-specific diseases. Patient-specific iPS cells may contribute to these concepts.

In terms of disease modeling using iPS cells, LQT2 is firstly noticed[13-15] because LQT2 is one of the most common genetic variants in long QT syndrome and there is no definitive therapy for LQT2. And drug discovery often failed at the expense of immense cost, due to the side effects related to HERG which is LQT2 associated gene product, following QT prolongation and lethal arrhythmia. First report showed the generation of LQT2 patient-specific iPS cells harboring A614V missense mutation in the *KCNH2* gene, which was previously shown to lead to a significant reduction of

IKr which is responsible for LQT2[15]. Detailed whole-cell patch-clamp and multi-electrode array (MEA) recordings revealed significant prolongation of the action potential duration in LQT2 iPS cell-derived cardiomyocytes. Voltage-clamp studies confirmed a significant reduction of the cardiac potassium current IKr. LQT2 iPS cell-derived cardiomyocytes also showed marked arrhythmogenicity, characterized by early-after depolarizations (EAD) and triggered arrhythmias. And calcium-channel blockers, K_{ATP}-channel openers and late sodium channel blockers ameliorate the disease phenotype in LQT2 iPS cell-derived cardiomyocyte. Second report showed the generation of LQT2 patient-specific iPS cells harboring G1681A missense mutation in the *KCNH2* gene, which was also previously shown to lead to a significant reduction of IKr[14]. MEA and patch-clamp recording showed prolonged field/action potential duration in LQT2 iPS cell-derived cardiomyocytes. LQT2 iPS cell-derived cardiomyocytes developed EADs when challenged with the E4031 (IKr blocker) and isoprenaline. Action potential duration and EAD were ameliorated by propranolol, nadolol, nicorandil and an activator of hERG, PD118057. The other report showed the generation of LQT2 patient-specific iPS cells harboring R176W missense mutation in the *KCNH2* gene[13]. The *KCNH2* R176W mutation is relatively common variant and was reported to have the frequency of 0.5% in apparently healthy individuals. Although there were some reports showed that this mutation was related to long QT syndrome, the majority of these individuals were completely asymptomatic and unaware of their carrier status, as is the case with this patient. In heterologous expression system, R176W reduced hERG tail current density by ~75%, but upon coexpression with wild type the difference in current densities was nullified. But the action potential duration of LQT2 iPS cell-derived cardiomyocytes was significantly longer than that of control, and IKr density of the LQT2 iPS cell-derived cardiomyocytes was significantly reduced. Consistent with clinical observations, the LQT2 iPS cell-derived cardiomyocytes demonstrated a more pronounced inverse correlation between the beating rate and repolarization time compared with control cells. Additionally, LQT2 iPS cell-derived cardiomyocytes were more sensitive than controls to potentially arrhythmogenic drugs, including sotalol, and demonstrated arrhythmogenic electrical activity.

In this study we chose a patient with a novel mutation in the *KCNH2* G603D. Patient showed QT interval prolongation but never showed any symptoms. To treat properly and prevent cardiac lethal arrhythmia, we believe it is valuable to generate experimental methods to predict how susceptible to lethal arrhythmia in various stimulations in those patients. Actually, many genomic variations such as many SNPs in each patient's genome affect disease manifestation even in the patients with major functional mutation and may be the cause of low penetrance for long QT syndrome[16]. So it is difficult to accurately predict disease susceptibility only by genomic information such as patient's mutation and SNPs. Patient-specific iPS cells have all genomic information encoded in patient's genome including mutation and all SNPs, and can be ideal disease models for the patients. Actually, each patient shows different disease phenotype and drug response, which is also partly due to patient genomic variation. In terms of personalized medicine, we can also try many notorious and beneficial drugs on patient-specific iPS cell-derived cardiomyocyte and predict disease susceptibility before the patient will use those drugs. To generate patient-specific disease models using iPS cells, we established the patient-specific iPS cells and confirmed the patient-specific iPS cells had the same mutation as the patient.

Acknowledgments

The authors thank all the laboratory members for their critical comments and helpful discussions.

References

1. Takahashi K, Yamanaka S. Induction of Pluripotent Stem Cells from Mouse Embryonic and Adult Fibroblast Cultures by Defined Factors. Cell. 2006; 126(4): 663-76.
2. Takahashi K, Tanabe K, Ohnuki M, et al. Induction of Pluripotent Stem Cells from Adult Human Fibroblasts by Defined Factors. Cell. 2007; 131(5): 861-72.
3. Seki T, Yuasa S, Oda M, et al. Generation of Induced Pluripotent Stem Cells from Human Terminally Differentiated Circulating T Cells. Cell Stem Cell. 2010; 7(1): 11-4.
4. Egashira T, Yuasa S, Fukuda K. Induced pluripotent stem cells in cardiovascular medicine. Stem Cells Int. 2011; 2011: 348960.
5. Yuasa S, Fukuda K. Recent advances in cardiovascular regenerative medicine: the induced pluripotent stem cell era. Expert Rev Cardiovasc Ther. 2008 Jul; 6(6): 803-10.
6. Yuasa S, Fukuda K. Cardiac regenerative medicine. Circ J. 2008; 72 Suppl A: A49-55.
7. Egashira T, Yuasa S, Suzuki T, et al. Disease characterization using LQTS-specific induced pluripotent stem cells. Cardiovasc Res. 2012 Sep 1; 95(4): 419-29.
8. Horigome H, Nagashima M, Sumitomo N, et al. Clinical characteristics and genetic background of congenital

long-QT syndrome diagnosed in fetal, neonatal, and infantile life: a nationwide questionnaire survey in Japan. Circ Arrhythm Electrophysiol. 2010 Feb; 3(1): 10-7.
9. Shimizu W, Horie M. Phenotypic manifestations of mutations in genes encoding subunits of cardiac potassium channels. Circ Res. 2011 Jun 24; 109(1): 97-109.
10. Giudicessi JR, Ackerman MJ. Potassium-channel mutations and cardiac arrhythmias—diagnosis and therapy. Nat Rev Cardiol. 2012; 9(6): 319-32.
11. Seki T, Yuasa S, Fukuda K. Generation of induced pluripotent stem cells from a small amount of human peripheral blood using a combination of activated T cells and Sendai virus. Nat Protoc. 2012 Apr; 7(4): 718-28.
12. Seki T, Yuasa S, Fukuda K. Derivation of Induced Pluripotent Stem Cells from Human Peripheral Circulating T Cells. Current Protocols in Stem Cell Biology: John Wiley & Sons, Inc.; 2011.
13. Lahti AL, Kujala VJ, Chapman H, et al. Model for long QT syndrome type 2 using human iPS cells demonstrates arrhythmogenic characteristics in cell culture. Dis Model Mech. 2012 Mar; 5(2): 220-30.
14. Matsa E, Rajamohan D, Dick E, et al. Drug evaluation in cardiomyocytes derived from human induced pluripotent stem cells carrying a long QT syndrome type 2 mutation. Eur Heart J. 2011 Apr; 32(8): 952-62.
15. Itzhaki I, Maizels L, Huber I, et al. Modelling the long QT syndrome with induced pluripotent stem cells. Nature. 2011; 471(7337): 225-9.
16. Priori SG, Schwartz PJ, Napolitano C, et al. Risk stratification in the long-QT syndrome. N Engl J Med. 2003 May 8; 348(19): 1866-74.

Induction of human cardiomyocyte-like cells from fibroblasts by defined factors

Rie Wada[a], Naoto Muraoka[a,b], Kohei Inagawa[a,b], Hiroyuki Yamakawa[a,b], Kazutaka Miyamoto[a,b], Taketaro Sadahiro[a,b], Tomohiko Umei[a], Ruri Kaneda[a,b], Tomoyuki Suzuki[b,c], Kaichiro Kamiya[c], Shugo Tohyama[b], Shinsuke Yuasa[b], Kiyokazu Kokaji[d], Ryo Aeba[d], Ryohei Yozu[d], Hiroyuki Yamagishi[e], Toshio Kitamura[f], Keiichi Fukuda[b], and Masaki Ieda[a,b,g,1]

[a]Department of Clinical and Molecular Cardiovascular Research and [b]Department of Cardiology, School of Medicine, Keio University, Tokyo 160-8582, Japan; [c]Department of Cardiovascular Research, Research Institute of Environmental Medicine, Nagoya University, Nagoya 464-8601, Japan; [d]Division of Cardiovascular Surgery and [e]Department of Pediatrics, School of Medicine, Keio University, Tokyo 160-8582, Japan; [f]Division of Cellular Therapy, Institute of Medical Science, University of Tokyo, Tokyo 108-8639, Japan; and [g]Japan Science and Technology Agency CREST, Tokyo 160-8582, Japan

Edited by Margaret Buckingham, Pasteur Institute, Paris, France, and approved June 11, 2013 (received for review March 6, 2013)

Heart disease remains a leading cause of death worldwide. Owing to the limited regenerative capacity of heart tissue, cardiac regenerative therapy has emerged as an attractive approach. Direct reprogramming of human cardiac fibroblasts (HCFs) into cardiomyocytes may hold great potential for this purpose. We reported previously that induced cardiomyocyte-like cells (iCMs) can be directly generated from mouse cardiac fibroblasts in vitro and vivo by transduction of three transcription factors: Gata4, Mef2c, and Tbx5, collectively termed GMT. In the present study, we sought to determine whether human fibroblasts also could be converted to iCMs by defined factors. Our initial finding that GMT was not sufficient for cardiac induction in HCFs prompted us to screen for additional factors to promote cardiac reprogramming by analyzing multiple cardiac-specific gene induction with quantitative RT-PCR. The addition of Mesp1 and Myocd to GMT up-regulated a broader spectrum of cardiac genes in HCFs more efficiently compared with GMT alone. The HCFs and human dermal fibroblasts transduced with GMT, Mesp1, and Myocd (GMTMM) changed the cell morphology from a spindle shape to a rod-like or polygonal shape, expressed multiple cardiac-specific proteins, increased a broad range of cardiac genes and concomitantly suppressed fibroblast genes, and exhibited spontaneous Ca^{2+} oscillations. Moreover, the cells matured to exhibit action potentials and contract synchronously in coculture with murine cardiomyocytes. A 5-ethynyl-2′-deoxyuridine assay revealed that the iCMs thus generated do not pass through a mitotic cell state. These findings demonstrate that human fibroblasts can be directly converted to iCMs by defined factors, which may facilitate future applications in regenerative medicine.

cell fate conversion | regeneration | cardiogenesis

Cardiovascular disease remains a leading cause of death worldwide, for which current therapeutic regimens remain limited. Given that adult human hearts have little regenerative capacity after injury, the demand is high for cardiac regenerative therapy. The recent discovery of induced pluripotent stem cells (iPSCs) allows the direct generation of specific cell types from differentiated somatic cells by overexpression of lineage-specific factors.

Several previous studies have demonstrated that such direct lineage reprogramming can yield a diverse range of cell types, including pancreatic β cells, neurons, neural progenitors, blood progenitors, and hepatocyte-like cells (1–5). We previously reported that a minimum mixture of three cardiac-specific transcription factors—Gata4, Mef2c, and Tbx5 (GMT)—directly induced cardiomyocyte-like cells (iCMs) from mouse fibroblasts in vitro (6). Following our report, three other groups also reported generation of functional cardiomyocytes from mouse fibroblasts with various combinations of transcription factors, either with GMT plus Hand2 (GHMT) or Mef2c, Myocd, and Tbx5 or using microRNAs (7–9). Although full reprogramming into beating cardiomyocytes was not efficient in vitro (10, 11), gene transfer of GMT or GHMT into mouse hearts generated new cardiomyocytes from endogenous cardiac fibroblasts and improved cardiac function after myocardial infarction (7, 12, 13). The foregoing studies suggest that direct cardiac reprogramming may be a useful therapeutic approach for regenerative purposes, and that identification of reprogramming factors in human cells is important for the development of this technology (14–16).

In the present study, we sought to generate cardiomyocytes directly from postnatal human fibroblasts. We found that GMT was not sufficient for cardiac reprogramming in human cells. We then screened additional reprogramming factors for their ability to induce cardiac reprogramming by analyzing multiple cardiac gene induction, and found that the addition of Mesp1 and Myocd to GMT was able to generate cardiomyocyte-like cells from human fibroblasts in vitro.

Results

Gata4, Mef2c, Tbx5, Mesp1, and Myocd Induce Multiple Cardiac Gene Expression in Human Cardiac Fibroblasts. We first developed a culture system for human cardiac fibroblasts (HCFs) following our mouse cardiac fibroblast isolation protocol. Human atrial tissues were obtained from 36 patients (age 1 mo to 80 y; average age, 35 y) undergoing cardiac surgery with informed consent following the guidelines of the Keio University Ethics Committee. The $Thy1^+/CD31^-$ FACS-sorted fibroblasts did not express cardiomyocyte or cardiac progenitor cell (CPC) genes, but did express fibroblast genes on quantitative RT-PCR (qRT-PCR) analysis (Fig. S1 *A–C*). HCFs expressed fibroblast proteins, vimentin, and fibronectin, but not markers of cardiomyocytes, CPCs, smooth muscle cells, or endothelial cells (Fig. 1*A* and Fig. S1*D*). The antibody immunoreactivities were confirmed in the positive controls (Fig. S1*E*). FACS analyses also demonstrated that the HCF population did not contaminate cardiomyocytes (Fig. 1*B*).

For transduction, we first used the sequential lentivirus/ecotropic retrovirus infection following the iPSC generation protocol from human dermal fibroblasts (HDFs) (17). The transduction efficiency was <20% in HCFs (Fig. 1*C*). We then directly infected HCFs using other types of retroviruses, produced by PLAT-A cells and PLAT-GP cells (18). We achieved high transduction efficiency

Author contributions: M.I. designed research; R.W., N.M., K.I., K.M., T. Suzuki, S.Y., R.A., and M.I. performed research; T. Sadahiro, T.U., S.T., K. Kokaji, R.Y., and T.K. contributed new reagents/analytic tools; H. Yamakawa, R.K., T. Suzuki, K. Kamiya, H. Yamagishi, K.F., and M.I. analyzed data; and M.I. wrote the paper.

The authors declare no conflict of interest.

This article is a PNAS Direct Submission.

[1]To whom correspondence should be addressed. E-mail: mieda@z8.keio.jp.

This article contains supporting information online at www.pnas.org/lookup/suppl/doi:10.1073/pnas.1304053110/-/DCSupplemental.

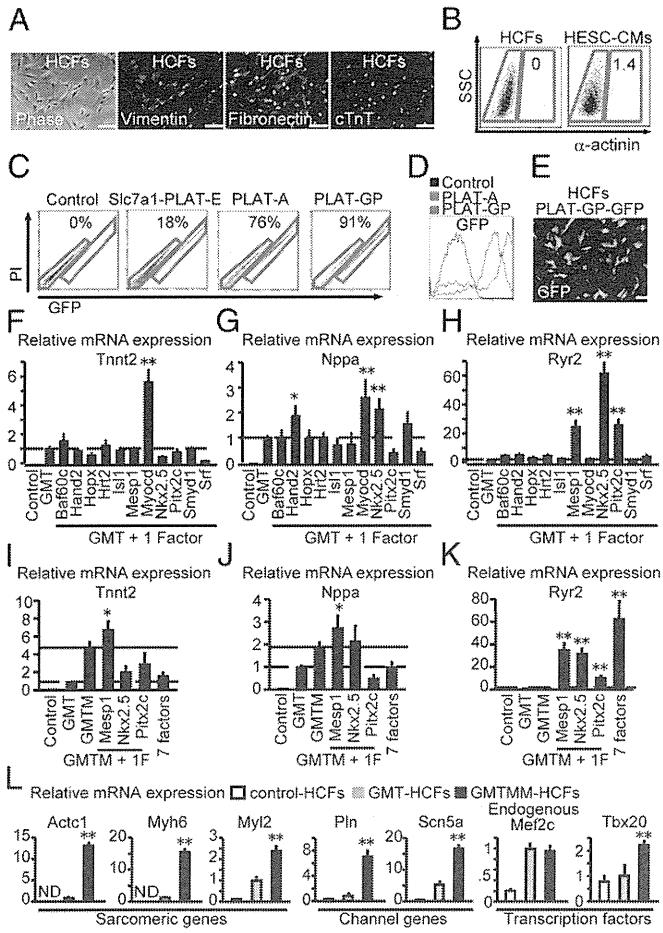

Fig. 1. Gata4, Mef2c, Tbx5, Mesp1, and Myocd induce cardiac gene expression in HCFs. (*A*) Morphology and characterization of HCFs by phase-contrast imaging, with vimentin, fibronectin, and cTnT immunostaining [passage number 1 (P1) HCFs, 57-y-old patient; $n = 3$]. The antibody immunoreactivities were confirmed in HESC-CMs (Fig. S1*E*). (*B*) FACS analysis for α-actinin$^+$ cells (HESC-CMs as a positive control) showed no expression in HCFs (P1 HCFs, 58-y-old patient; $n = 3$). (*C*) FACS analysis of the HCFs transduced by sequential infection of Slc7a1 lentivirus and ecotropic GFP retrovirus (Slc7a1-PLAT-E), amphotropic GFP retrovirus produced by PLAT-A cells (PLAT-A), and pantropic GFP retrovirus produced by PLAT-GP cells (PLAT-GP) (P1 HCFs from patients aged 1 mo and 50 y; $n = 4$). (*D*) Histogram of GFP intensity in the transduced HCFs determined by FACS analysis (P1 HCFs from 50-y-old patient; $n = 3$). GFP expression was high in cells transduced with retrovirus produced by PLAT-GP. (*E*) Image of HCFs infected by the GFP retrovirus produced by PLAT-GP. (*F–H*) mRNA expression of cardiac genes (*Tnnt2*, *Nppa*, and *Ryr2*) in HCFs transduced with GMT plus individual factors as determined by qRT-PCR after 1 wk of transduction (P1 HCFs, 71-y-old patient; $n = 3$). Data were normalized against the GMT values. See also Fig. S2 *A–E* and Movie S1. (*I–K*) The mRNA expression of cardiac genes in HCFs transduced with GMTM plus Mesp1, Nkx2.5, Pitx2c, or all three genes was determined by qRT-PCR after 1 wk of transduction (P1 HCFs, 59-y-old patient; $n = 3$). Data were normalized against the GMT values. (*L*) Multiple cardiac genes were up-regulated in GMTMM-HCFs after 1 wk of transduction (P1 HCFs, 2-y-old patient; $n = 3$). Representative data are shown in each panel. All data are presented as mean ± SD. $^*P < 0.05$; $^{**}P < 0.01$ vs. relevant control. (Scale bars: 100 μm.)

(>90%) using the pantropic retrovirus from PLAT-GP cells, and used this virus in subsequent experiments (Fig. 1 *C–E*).

We next transduced HCFs with a mixture of GMT retroviruses. The GMT overexpression induced very few α-actinin$^+$ cells, suggesting that this mixture is insufficient for human cardiac reprogramming (Fig. 2*A*). To identify reprogramming factors, we screened an additional 11 factors for use in combination with GMT and analyzed the induction of multiple cardiac genes by qRT-PCR after 1 wk of transduction. Of these 11 factors, only Myocd strongly induced *Tnnt2* expression (Fig. 1*F*). Myocd also induced *Nppa*, but did not induce *Ryr2* (ryanodine receptor 2). In contrast, Mesp1, Nkx2.5, and Pitx2c strongly induced *Ryr2* expression (Fig. 1 *G* and *H*).

Consistent with our qRT-PCR results, FACS analysis and immunocytochemistry demonstrated that the addition of Myocd to GMT increased the expression of sarcomere proteins α-actinin and cTnT in HCFs compared with Mesp1. In contrast, threefold more cells exhibited spontaneous Ca^{2+} oscillations by transduction of GMTMesp1 compared with GMTMyocd after 4 wk of culture (Fig. S2 *A–E* and Movie S1).

We next investigated whether the addition of Mesp1, Nkx2.5, or Pitx2c to GMT and Myocd could induce multiple cardiac gene expression. We found that Nkx2.5 and Pitx2c inhibited *Tnnt2* mRNA expression, but that addition of Mesp1 up-regulated all three cardiac genes (Fig. 1 *I–K*). Moreover, transduction of Gata4, Mef2c, Tbx5, Mesp1, and Myocd (GMTMM) up-regulated the expression of a panel of cardiac genes related to different functions, including sarcomere structure, ion channels, and transcription factors, compared with GMT or mock infection, suggesting a more comprehensive reprogramming by GMTMM than by GMT (Fig. 1*L*).

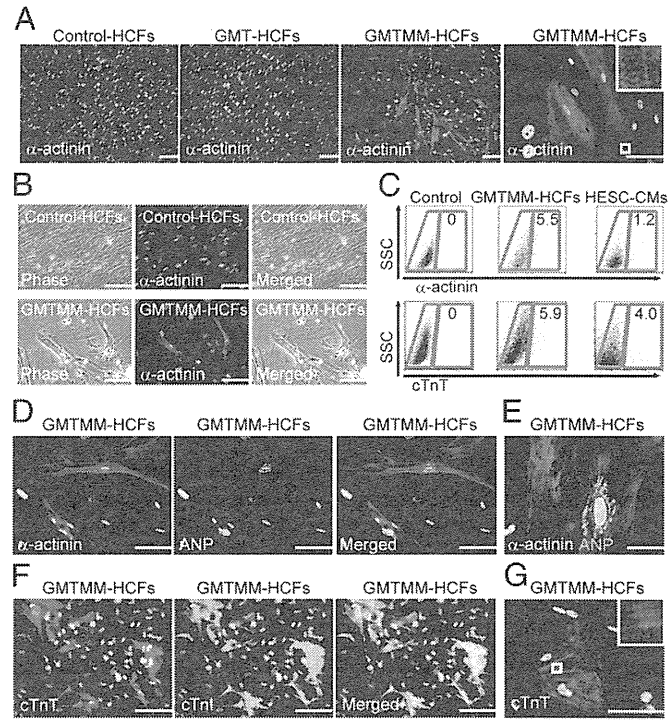

Fig. 2. Generation of cardiomyocyte-like cells from HCFs with GMTMM. (*A*) Immunostaining for α-actinin and DAPI in HCFs and GMT- or GMTMM-transduced HCFs at 4 wk after transduction (P1 HCFs, 3-y-old patient; $n = 4$). Note that GMTMM induced abundant and strong α-actinin expression. (*Inset*) High-magnification view of the area in the white box showing sarcomeric organization (see Fig. S1*E* for a positive control). (*B*) Morphology of mock- and GMTMM-infected HCFs by phase-contrast imaging and with α-actinin immunostaining (P1 HCFs, 57-y-old patient; $n = 3$). (*C*) Quantitative data of α-actinin$^+$ (P1 HCFs, 3-mo-old patient; $n = 3$) and cTnT$^+$ (P1 HCFs, 5-mo-old patient; $n = 3$) cells in GMTMM-HCFs and HESC-CMs ($n = 3$). (*D* and *E*) GMTMM-HCFs expressed both α-actinin and ANP at 4 wk after transduction (P1 HCFs, 5-y-old patient; $n = 2$). ANP was expressed at the perinuclear site. (*F* and *G*) Induced cardiomyocyte-like cells expressed cTnT and cTnI at 8 wk after GMTMM transduction (P1 HCFs, 5-y-old patient; $n = 2$). (Inset) High-magnification view representing the area in the white box. Representative data are shown in each panel. (Scale bars: 100 μm in *A*, *B*, *D*, *F*, and *G*; 50 μm in *E*.)